CMS Draft Analysis Note

The content of this note is intended for CMS internal use and distribution only

2018/09/05
Head Id: 473951
Archive Id: 473980M
Archive Date: 2018/09/05
Archive Tag: trunk

Search for new physics via top quark production in dilepton final state at 13 TeV

B. Clerbaux[1], W. Fang[2], X. Gao[2], and R. Goldouzian[1]

[1] IIHE-ULB, Université Libre de Bruxelles, Brussels, Belgium
[2] School of Physics and Nuclear energy engineering, Beihang University, China (also at IIHE-ULB, Université Libre de Bruxelles, Brussels, Belgium)

Abstract

We search for new physics in top-quark interactions, using an effective field theory approach. We consider single top quark production in association with a W boson, and top-quark pair production in dilepton final states using data from proton-proton collisions at 13 TeV. The dataset corresponds to an integrated luminosity of 35.9 fb^{-1} and was collected in 2016 by the CMS detector.

Contents

1 Introduction . . . 2
1.1 Effective field theory approach . . . 2
1.2 Global fit of top quark effective theory . . . 4
1.3 Effective couplings versus anomalous couplings . . . 4
2 Signal production procedure and cross section calculation . . . 5
2.1 TopEffTh . . . 6
2.2 dim6top_LO_UFO_each_coupling_order . . . 7
2.3 Final cross sections . . . 7
3 Search startegy . . . 7
4 Datasets and Monte Carlo Samples . . . 13
4.1 Signal sample and cross section calculation . . . 13
5 Triggers . . . 13
6 Event reconstruction and object identification . . . 13
7 Background predictions . . . 14
8 Signal extraction . . . 14
8.1 Data/MC comparison for MVA input variables . . . 18
9 Systematic uncertainties . . . 22
10 Results . . . 23
10.1 Limit setting procedure . . . 23
10.2 Exclusion limits on C_G effective coupling . . . 24
10.3 Exclusion limits on C_{tG}, $C_{\phi q}$ and C_{tW} effective couplings . . . 26
10.4 Exclusion limits on C_{uG} and C_{cG} effective couplings . . . 29
11 Summary . . . 31

Important notes for this version of note

- This note is supported by AN-17-132 for details about the trigger, object selection, event selection, SM background estimation. In this note we only focus on new physics search.
- Main changes in this version of the note compared to the last version of note.

1. Scale variation uncertainties on the cross sections are taken into account.
2. Results are updated after reweighting $t\bar{t}$ events as a function of top p_T.
3. In order to follow new released TOPLHC framework for EFT interpretations, g_s is removed from FCNC Lagrangian. NLO k-factor is added to FCNC cross sections and a small bug is fixed.
4. Adding 3% constant error to take into account the effect of acceptance*efficiency difference for O_G.

1 Introduction

1.1 Effective field theory approach

Due to its large mass, close to the electroweak symmetry breaking scale, the top quark is expected to play an important role in new physics searches. If the new physics scale is in the available energy range of the LHC, the existence of new physics could be directly observed via the production of new particles. Otherwise, new physics could affect standard model (SM) interactions indirectly, through modifications of SM couplings or enhancements of rare SM processes. In the latter case, it is useful to introduce a model independent approach to parametrize and to constrain possible deviations from SM predictions, independently of the fundamental theory of new physics.

An effective field theory (EFT) approach is followed to search for new physics in the top quark sector in the dilepton final states. In references [1, 2] all dimension-six operators that contribute to the top quark pair production ($t\bar{t}$) and the single top quark production in association with a W boson (tW) are investigated. The operators and related effective Lagrangians which are relevant for dilepton final states can be written as [3]:

$$O_{\phi q}^{(3)} = (\phi^+\tau^I D_\mu \phi)(\bar{q}\gamma^\mu\tau^I q), \quad L_{eff} = \frac{C_{\phi q}^{(3)}}{\sqrt{2}\Lambda^2} g v^2 \bar{b}\gamma^\mu P_L t W_\mu^- + h.c., \tag{1}$$

$$O_{tW} = (\bar{q}\sigma^{\mu\nu}\tau^I t)\tilde{\phi}W_{\mu\nu}^I, \quad L_{eff} = -2\frac{C_{tW}}{\Lambda^2} v\bar{b}\sigma^{\mu\nu}P_R t\partial_\nu W_\mu^- + h.c., \tag{2}$$

$$O_{tG} = (\bar{q}\sigma^{\mu\nu}\lambda^A t)\tilde{\phi}G_{\mu\nu}^A, \quad L_{eff} = \frac{C_{tG}}{\sqrt{2}\Lambda^2} v\left(\bar{t}\sigma^{\mu\nu}\lambda^A t\right) G_{\mu\nu}^A + h.c., \tag{3}$$

$$O_G = f_{ABC}G_\mu^{A\nu}G_\nu^{B\rho}G_\rho^{C\mu}, \quad L_{eff} = \frac{C_G}{\Lambda^2} f_{ABC}G_\mu^{A\nu}G_\nu^{B\rho}G_\rho^{C\mu} + h.c., \tag{4}$$

$$O_{u(c)G} = (\bar{q}\sigma^{\mu\nu}\lambda^A t)\tilde{\phi}G_{\mu\nu}^A, \quad L_{eff} = \frac{C_{u(c)G}}{\sqrt{2}\Lambda^2} v\left(\bar{u}\left(\bar{c}\right)\sigma^{\mu\nu}\lambda^A t\right) G_{\mu\nu}^A + h.c., \tag{5}$$

where $C_{\phi q}^{(3)}$, C_{tW}, C_{tG}, C_G and $C_{u(c)G}$ stand for the dimensionless Wilson coefficients, also called as the effective couplings. The variable Λ represents the energy scale beyond which new

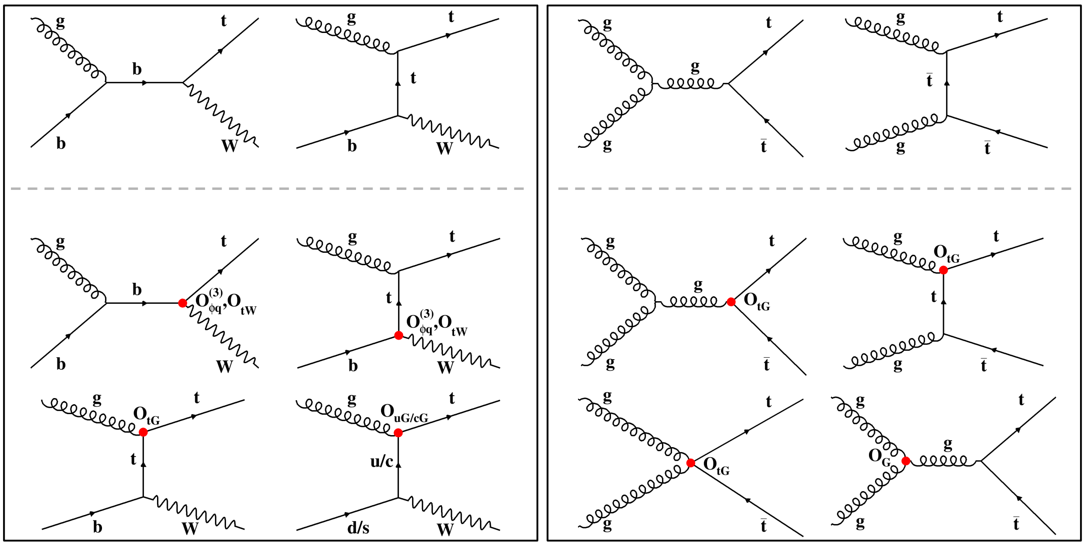

Figure 1: Representative Feynman diagrams for the tW (left panel) and $t\bar{t}$ (right panel) production at leading order. The top row gives the SM diagrams, the middle and bottom rows present diagrams corresponding to the $O_{\phi q}^{(3)}$, O_{tW},O_{tG}, O_G and $O_{u/cG}$ contributions.

physics becomes relevant. The detailed description of the operators is given in references [1, 2]. The operators $O_{\phi q}^{(3)}$ and O_{tW} modify the SM W boson-top-b quark (Wtb) interaction, and its effect can be probed in both top quark decays and single top quark production. The operator O_{tG}, called as the chromomagnetic dipole moment operator of the top quark, can be investigated in both tW and top quark pair production. The triple gluon field strength operator O_G represents the only genuinely gluonic CP conserving term which can appear at dimension 6 within an effective strong interaction Lagrangian [4]. The operators O_{uG} and O_{cG} lead to flavor changing neutral current (FCNC) interactions of top quark and contribute to the tW production. Representative Feynman diagrams for new physics contributions in the tW and $t\bar{t}$ production are shown in Fig. 1. It should be noted that the O_{tW} and O_{tG} operators with imaginary coefficient lead to CP-violating effects. In this analysis we only probe CP-even dimension six operators to top quark production.

Several searches for new physics in the top quark sector including new non-SM couplings have been performed at the Tevatron and LHC colliders. Results can be interpreted in two ways. Most of the previous analyses followed the anomalous coupling approach in which SM interactions are extended for possible new interactions. In this article, the EFT framework with effective couplings is used for the interpretation of the results. Constraints obtained on anomalous couplings can be easily translated to effective coupling bounds [1, 5]. A variety of limits have been set on the Wtb top quark anomalous coupling through single top quark *t*-channel production and measurements of the W boson polarization from top quark decay by the D0 [5], ATLAS [6, 7] and CMS [8, 9] collaborations. Direct limits on the top chromomagnetic dipole moment have been obtained by the CMS collaboration at 7 TeV using top quark pair events [10]. Searches for top quark FCNC interactions have been performed at Tevatron [11, 12] and at LHC [8, 13] via single top production and limits are set on related anomalous couplings.

In this analysis, a search for new physics in top quark production using an EFT framework is reported. Final states with two isolated leptons (electrons or muons) in association with jets identified as originated from the fragmentation of a b quark ("b-jets") are analysed. The search is sensitive to new physics contributions to the $t\bar{t}$ and tW production, and the six effective

couplings, $C_{\phi q}^{(3)}$, C_{tW}, C_{tG}, C_G, C_{uG} and C_{cG} are constrained independently. The search for new physics in the tW process is performed for the first time. The search utilizes 35.9 fb^{-1} of proton-proton collision data collected by the CMS experiment in 2016 at a centre-of-mass energy of 13 TeV.

1.2 Global fit of top quark effective theory

In ref. [14], a global fit of top quark effective field theory is performed to experimental data and constrains are set. In figure 2, those constrains are shown.

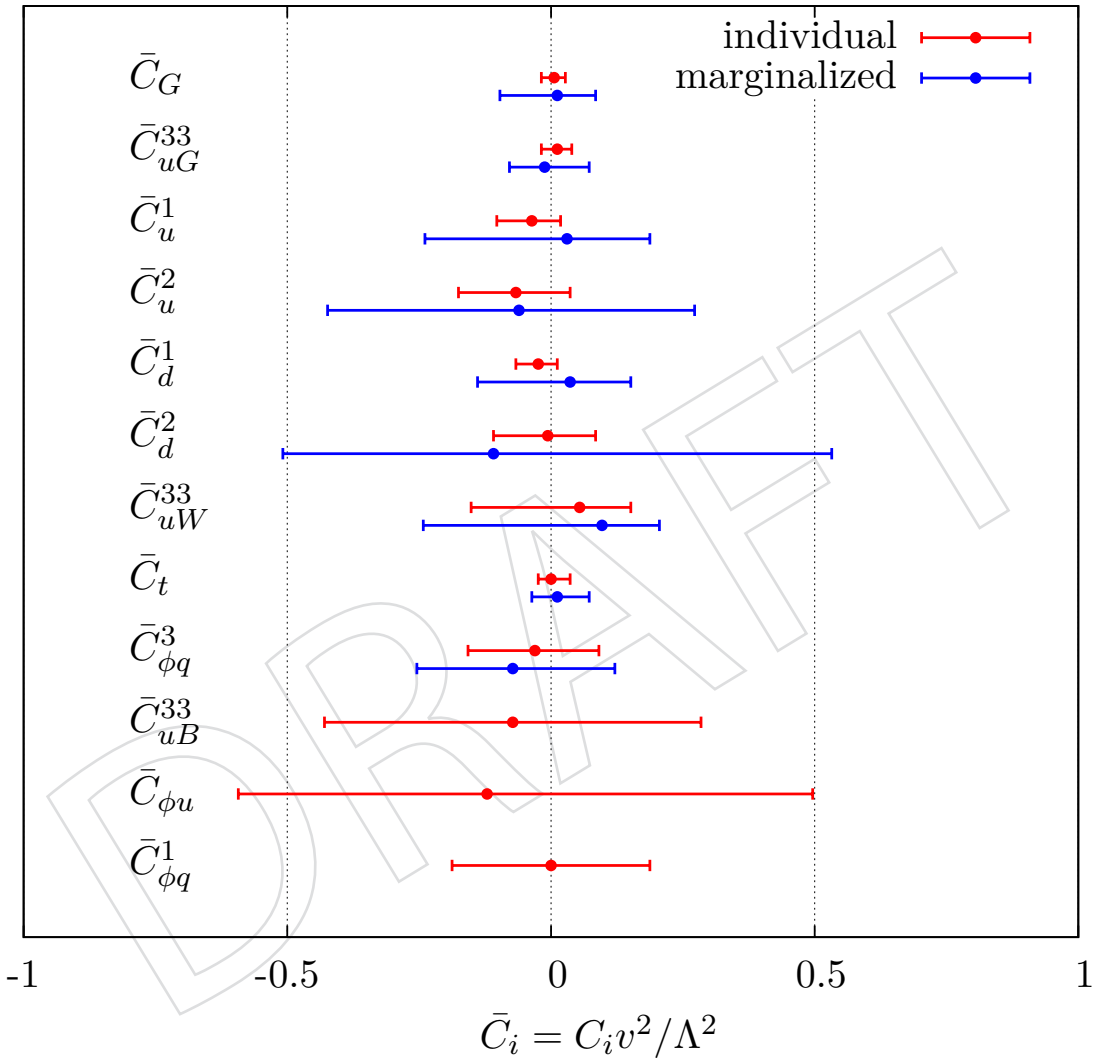

Figure 2: This figure is copied from ref. [14]. 95% confidence intervals for the dimension-six operators that we consider here, with all remaining operators set to zero (red) and marginalised over (blue). In cases where there are constraints on the same operator from different classes of measurement, the strongest limits are shown here.

1.3 Effective couplings versus anomalous couplings

As a matter of fact, a number of analyses including nonstandard couplings have been performed in at high-energy hadron colliders ever since more than a decade ago. However, the couplings used there were not always the same.

In the anomalous coupling approach, SM Lagrangian is extended in a way to consider more general interactions. For example, in ref [5], combination of searches for anomalous top quark couplings in D0 collaboration is presented in which Wtb anomalous couplings are considered. They have looked for physics beyond the SM in the form of right-handed vector couplings or left- or right-handed tensor couplings:

$$\begin{aligned}\mathcal{L} &= \frac{g}{\sqrt{2}}\bar{b}\gamma^{\mu}V_{tb}(f_V^L P_L + f_V^R P_R)tW_{\mu}^{-} \\ &\quad -\frac{g}{\sqrt{2}}\bar{b}\frac{i\sigma^{\mu\nu}q_{\nu}V_{tb}}{M_W}(f_T^L P_L + f_T^R P_R)tW_{\mu}^{-} + h.c.\,, \end{aligned} \tag{6}$$

where M_W is the mass of the W boson, q is its four-momentum, V_{tb} is the Cabibbo-Kobayashi-Maskawa matrix element, and $P_L = (1-\gamma_5)/2$ ($P_R = (1+\gamma_5)/2$) is the left-handed (right-handed) projection operator. In the SM, the left-handed vector coupling form factor is $f_V^L = 1$, the right-handed vector coupling form factor is $f_V^R = 0$, and the tensor coupling form factors are $f_T^L = f_T^R = 0$.

The mentioned anomalous coupling can be translated into the Wilson coefficients using the following equations (The detailed description of the operators and symbols is given in references [5, 15]):

$$\begin{aligned}|f_V^L| &= 1 + |C_{\phi q}^{(3)}|\frac{v^2}{V_{tb}\Lambda^2}\,, \\ |f_V^R| &= \frac{1}{2}|C_{\phi\phi}|\frac{v^2}{V_{tb}\Lambda^2}\,, \\ |f_T^L| &= \sqrt{2}|C_{bW}|\frac{v^2}{V_{tb}\Lambda^2}\,, \\ |f_T^R| &= \sqrt{2}|C_{tW}|\frac{v^2}{V_{tb}\Lambda^2}\,, \end{aligned} \tag{7}$$

Top anomalous couplings to the gluons can be parametrized by adding an effective term to the top-gluon gauge coupling,

$$\mathcal{L}_{\rm tg} = -g_s\bar{t}\gamma^{\mu}\frac{\lambda_a}{2}t\,G_{\mu}^a + \frac{g_s}{m_t}\bar{t}\sigma^{\mu\nu}(d_V + id_A\gamma_5)\frac{\lambda_a}{2}t\,G_{\mu\nu}^a\,, \tag{8}$$

with $G_{\mu\nu}^a$ ($a = 1,\ldots,8$) being the gluon field strength tensor, g_s the strong coupling constant, m_t the top mass and λ_a the Gell-Mann matrices. d_V and d_A are top chromomagnetic and chromoelectric dipole moments, respectively.

Top anomalous couplings to the gluons can be translated into the Wilson coefficients using the following equations

$$d_V = \frac{\sqrt{2}vm_t}{g_s\Lambda^2}\mathrm{Re}\,C_{tG}\,, \quad d_A = \frac{\sqrt{2}vm_t}{g_s\Lambda^2}\mathrm{Im}\,C_{tG}\,, \tag{9}$$

2 Signal production procedure and cross section calculation

One can write a general form of the cross section in the presence of the Wilson coefficients as:

$$\sigma = \sigma_{SM} + C_i\sigma_i^{(1)} + C_i^2\sigma_i^{(2)}\,, \tag{10}$$

where σ_{SM} is the SM cross section, "$C_i\sigma_i^{(1)}$" is the interference term between SM and new physics and "$C_i^2\sigma_i^{(2)}$" is the pure new physics term. In the following we check all available UFO models for top EFT interactions for finding the $\sigma_i^{(1)}$ and $\sigma_i^{(2)}$ factors.

2.1 TopEffTh

The TopEffTh model can be found in the *models* directory of MadGraph5 files. The only particularity to generate a process is the possibility to specify the order NP (which stands for New Physics) in addition to the usual QED and QCD order. NP is the maximum order in $1/\Lambda$, so in our case NP=2. Therefore, we can find the cross section of the interested processes as a function of effective couplings at leading order. The results are found with the following criteria: Λ = 1 TeV, m_t = 172.5, $\sqrt{s}$ = 13 TeV, PDF = 'NNPDF30' (LHAPDF6 code=263000) and the default dynamic factorization and renormalization scales in MG5 [16].

In order to find the cross section of $t\bar{t}$ and tW in the presence of the Wilson coefficients, we have performed the following steps

- tW/ttbar process is generated by Madgraph while all Wilson coefficient are present
- All Wilson coefficient are set to zero and cross section is calculated. This cross section is σ_{SM} at LO
- Imaginary part of a Wilson coefficient is set to a non-zero value while all other Wilson coefficient are set to zero and cross section is recalculated. This cross section is equal to $(\sigma_{SM} + C_i^2\sigma_i^{(2)})$. We extract B factor using σ_{SM} from previous step
- The real part of Wilson coefficient is set to a non-zero value while all other Wilson coefficient are set to zero and cross section is recalculated. This cross section is equal to $(\sigma_{SM} + C_i\sigma_i^{(1)} + C_i^2\sigma_i^{(2)})$. Using the results of last two steps, we can extract A factor
- We predict cross section for arbitrary value of Re(C_i) and compare with the result from generator to test the functional form of cross section

Following the steps mentioned above, we find:

$$\begin{aligned}\sigma_{LO}(pp \to tW^+ + pp \to \bar{t}W^-) &= \sigma_{SM}\,\text{pb} + (6.7\,\text{pb}\,C_{\phi q}^{(3)} - 4.45\,\text{pb}\,C_{tW} + 6.55\,\text{pb}\,C_{tG}) \\ &+ (0.21\,\text{pb}\,C_{\phi q}^{(3)^2} + 1\,\text{pb}\,C_{tW}^2 + 4.99\,\text{pb}\,C_{tG}^2) \end{aligned} \quad (11)$$

$$\begin{aligned}\sigma_{LO}(pp \to t\bar{t}) &= \sigma_{SM}\,\text{pb} + (274.1\,\text{pb}\,C_{tG} + 31.9\,\text{pb}\,C_G) \\ &+ (65.4\,\text{pb}\,C_{tG}^2 + 102.3\,\text{pb}\,C_G^2) \end{aligned} \quad (12)$$

One can parametrize the cross section of tW production via FCNC interaction as follows

$$\sigma^{FCNC}(pp \to tW \to lvblv) = 16.2C_{uG}^2 + 4.6C_{cG}^2(pb) \quad (13)$$

Due to the larger parton distribution function (PDF) of d quark (valance quark) in proton comparing to s quark (sea quarks), the contribution of the tug effective coupling to the cross section is larger than the contribution of tcg effective coupling. In order to translate the limits on the FCNC effective couplings to the constrains on related branching ratios, we use:

$$\Gamma_{FCNC}(t \to qG) = 0.033 C_{qG}^2 \ \ GeV \ \ (m_{top} = 172.5, \Lambda = 1 TeV) \quad (14)$$
$$\Gamma_{SM}(t \to Wb) = 1.33 \ \ GeV \ \ (m_{top} = 172.5) \quad (15)$$
$$BR(t \to qG) = \Gamma_{FCNC}/\Gamma_{SM} = 0.025 C_{qG}^2 \ \ GeV \ \ (m_{top} = 172.5, \Lambda = 1 TeV) \quad (16)$$

2.2 dim6top_LO_UFO_each_coupling_order

Recently, TOP LHC working group has proposed common standards and prescriptions for the effective-field-theory interpretation of top-quark measurements at the LHC [17]. They have also provided a new UFO file for generating events at leading order. One of the important features of this model is that one can access to the factors A and B directly without doing the calculation explained in previous section. Using this new UFO file we find:

$$\begin{aligned} \sigma_{LO}(pp \to tW^+ + pp \to \bar{t}W^-) &= 55.24\,\text{pb} + (6.69\,\text{pb}\, C_{\phi q}^{(3)} - 4.71\,\text{pb}\, C_{tW} + 3.32\,\text{pb}\, C_{tG}) \\ &+ (0.20\,\text{pb}\, C_{\phi q}^{(3)^2} + 1.29\,\text{pb}\, C_{tW}^2 + 1.24\,\text{pb}\, C_{tG}^2) \end{aligned} \quad (17)$$

$$\begin{aligned} \sigma_{LO}(pp \to t\bar{t}) &= 491.3\,\text{pb} + 274.1\,\text{pb}\, C_{tG}) \\ &+ 65.4\,\text{pb}\, C_{tG}^2 \end{aligned} \quad (18)$$

The $\sigma_i^{(1)}$ and $\sigma_i^{(2)}$ factors in equations 17 and 18 are similar to what is found in equations 11 and 12 for $C_{\phi q}^{(3)}$, C_{tW} couplings. The $\sigma_i^{(1)}$ ($\sigma_i^{(2)}$) factor is 2 (4) times less for C_{tG} coupling. The C_G coupling is not included in this UFO model. After investigation, it is found that an extra factor of 2 is set in the Lagrangian for TopEffTh model. It is in line 230 of [18].

QLbar[sp, ii, 3, cc1].uR [sp2, 3, cc2]I/2*(Ga[mu,sp,sp1]Ga[nu,sp1,sp2]-Ga[nu,sp,sp1]Ga[mu,sp1,sp2])
Phibar[jj] Eps[ii, jj] 2 *T[aa,cc1,cc2] FS[G,mu,nu,aa]];

2.3 Final cross sections

In the literature, $t\bar{t}$ and tW cross sections as a function of EFT couplings are calculated at next to leading order in QCD [19, 20]. We use cross sections obtained from 'TopEffTh' and k-factors obtained from authors in [19, 20] as are summarized in table 1.

3 Search startegy

The operator $O_{\phi q}^{(3)}$ has interaction the same as the SM Wtb interaction. Therefore, it does not affect any distributions, and is impossible to detect in angular distributions of top-quark decays. The distributions of different kinematic variables are checked comparing the SM Wtb and beyond SM $O_{\phi q}^{(3)}$ interaction. The distributions of different kinematic variables are shown in Fig 3.

After investigating the distribution of many kinematic variables when the O_{tG} or O_{tW} operators are present, we conclude that the kinematic distributions in both processes, tW and $t\bar{t}$ production and top decay, are similar and the effects are not big enough to be observed. In figure 4

Table 1: Cross sections for $t\bar{t}$ and tW production [in pb] for the various effective couplings for Λ = 1 TeV. The respective available K-factors are also shown.

Channel	Variable	C_G	$C_{\phi q}^{(3)}$	C_{tW}	C_{tG}	C_{uG}	C_{cG}
$t\bar{t}$	$\sigma_i^{(1)-LO}$	31.9	-	-	137	-	-
	$\sigma_i^{(1)-NLO}/\sigma_i^{(1)-LO}$	-	-	-	1.48 [19]	-	-
	$\sigma_i^{(2)-LO}$	102.3	-	-	16.4	-	-
	$\sigma_i^{(2)-NLO}/\sigma_i^{(2)-LO}$	-	-	-	1.44 [19]	-	-
tW	$\sigma_i^{(1)-LO}$	-	6.7	-4.5	3.3	0	0
	$\sigma_i^{(1)-NLO}/\sigma_i^{(1)-LO}$	-	1.32 [20]	1.27 [20]	1.27 [20]	0	0
	$\sigma_i^{(2)-LO}$	-	0.2	1	1.2	16.2	4.6
	$\sigma_i^{(2)-NLO}/\sigma_i^{(2)-LO}$	-	1.31	1.18	1.06	1.27	1.27

and 5, the distributions of some variables with high discriminating power are shown for SM signal and BSM signal. So we consider the effects of the effective couplings only on the rate changes of $t\bar{t}$ and tW processes. After selection, $t\bar{t}$ events are dominant in all njet-mtag regions and it is not possible to observe small deviation to SM tW prediction by simple event counting method. Therefore, we will train an MVA to separate tW from $t\bar{t}$ events. Finaly, we will use MVA output to constrain $C_{\phi q}^{(3)}$, C_{tW}, and C_{tG} couplings.

As is mentioned in reference [4] and is shown in figure 6, few variables are different between SM $t\bar{t}$ production and BSM $t\bar{t}$ production due to the O_G operator. On the other hand, the difference between SM $t\bar{t}$ production and BSM $t\bar{t}$ production due to the O_G operator is not big enough to use them for discriminating between signal and background events. Therefore, we only focus on the rate changes of ttbar production because of the O_G operator and avoid using MVA (see section 10).

The tW production via the FCNC interactions does not interfere with the SM tW production. On the other hand, event kinematics can be distinguished from SM backgrounds because of different quarks in initial state. Therefore, we will train an MVA to discriminate between the tW FCNC signal and other SM backgrounds and will use both signal shape and rate to constrain FCNC effective couplings.

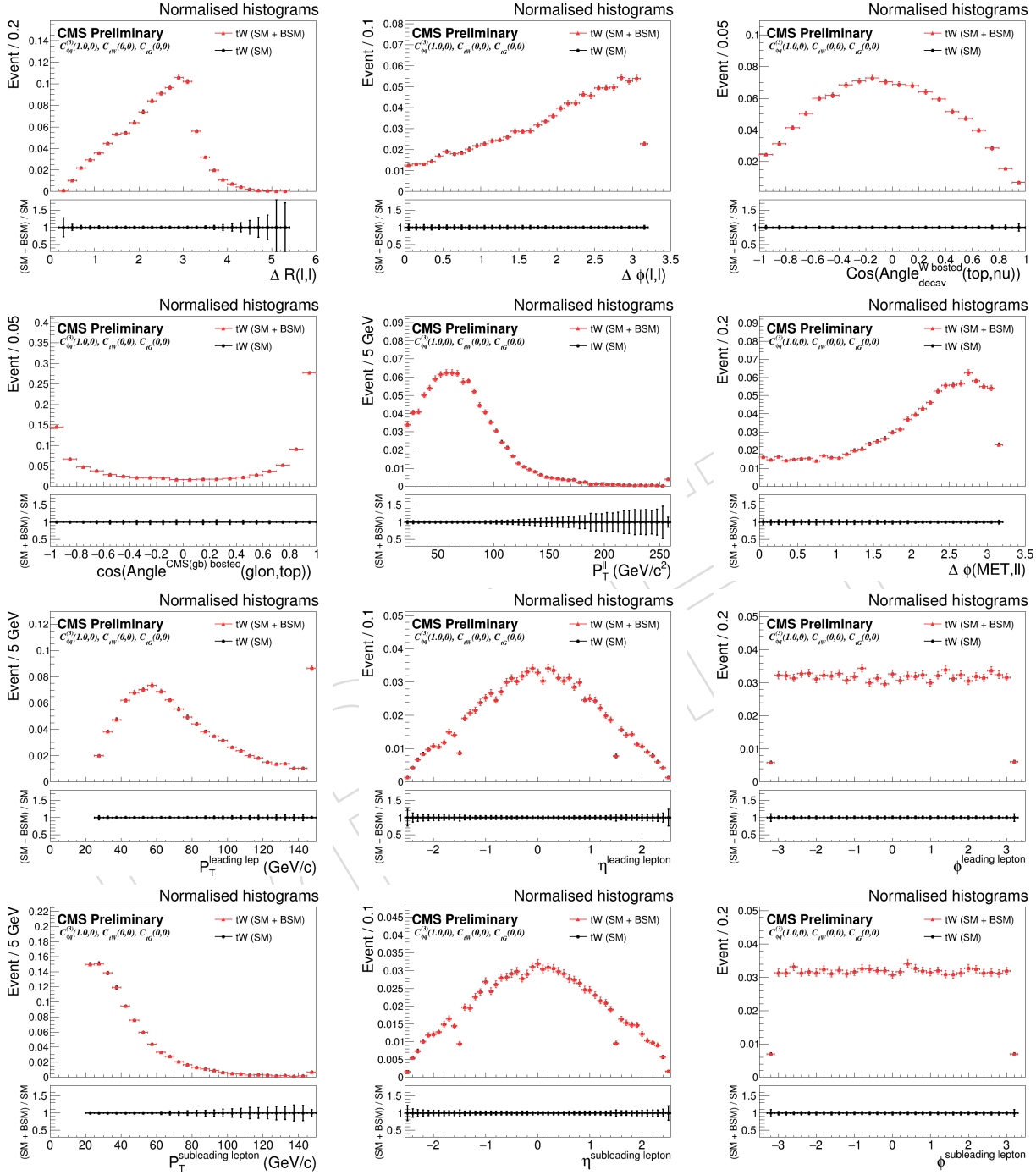

Figure 3: The distributions of some variables from operator $O_{\phi q}^{(3)}$

.

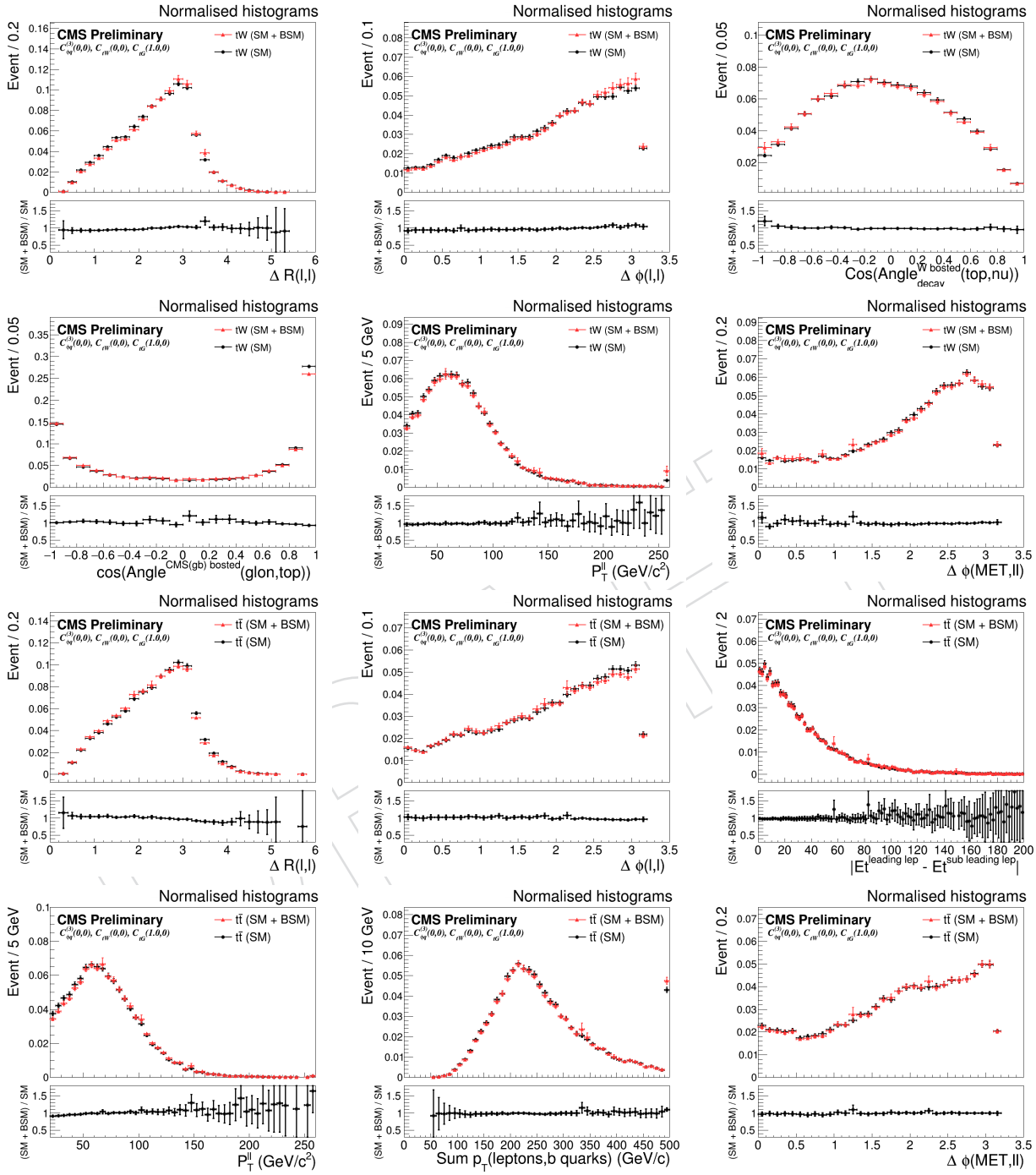

Figure 4: The distributions of some variables from operator O_{tG}

.

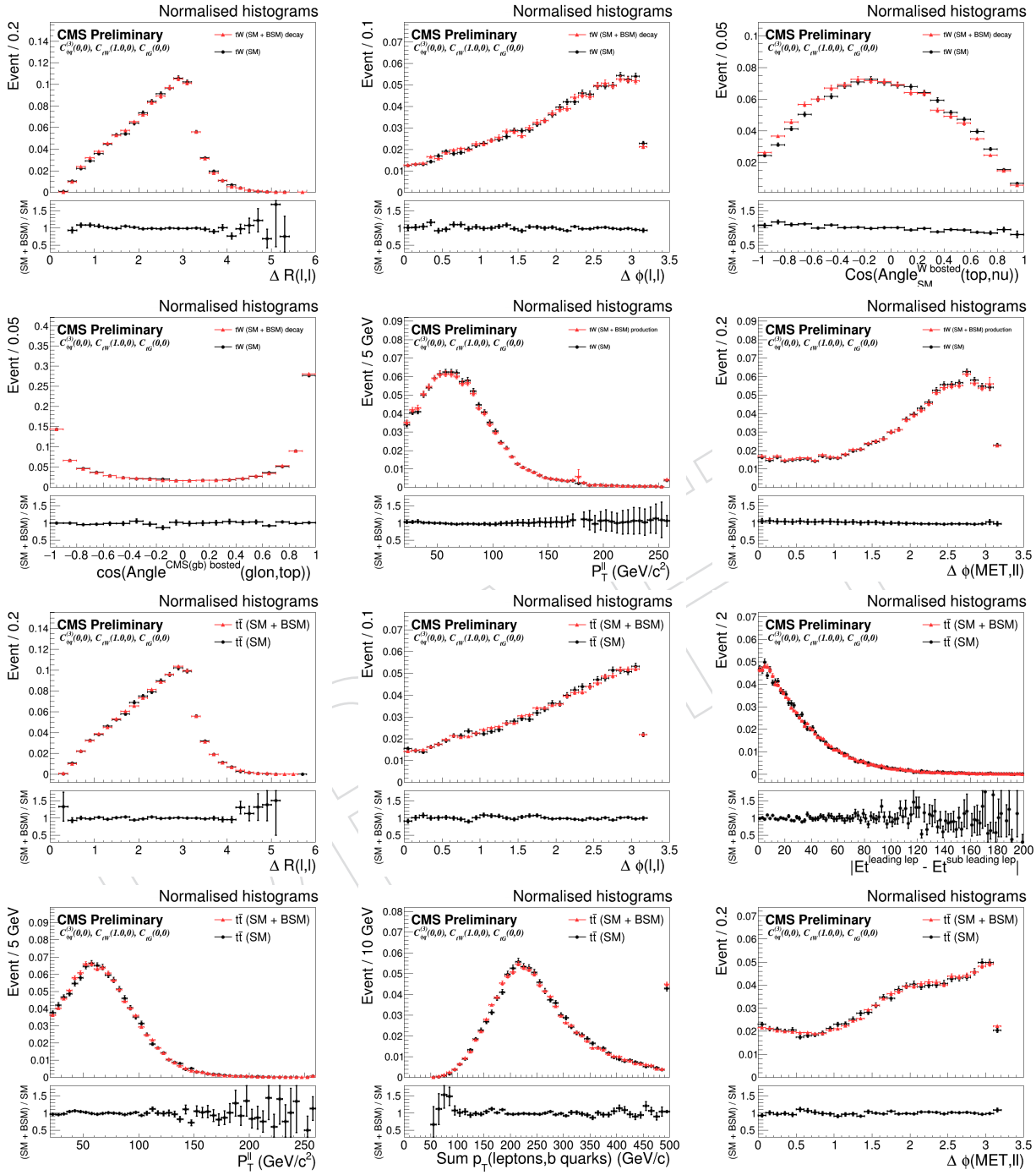

Figure 5: The distributions of some variables from operator O_{tW}

.

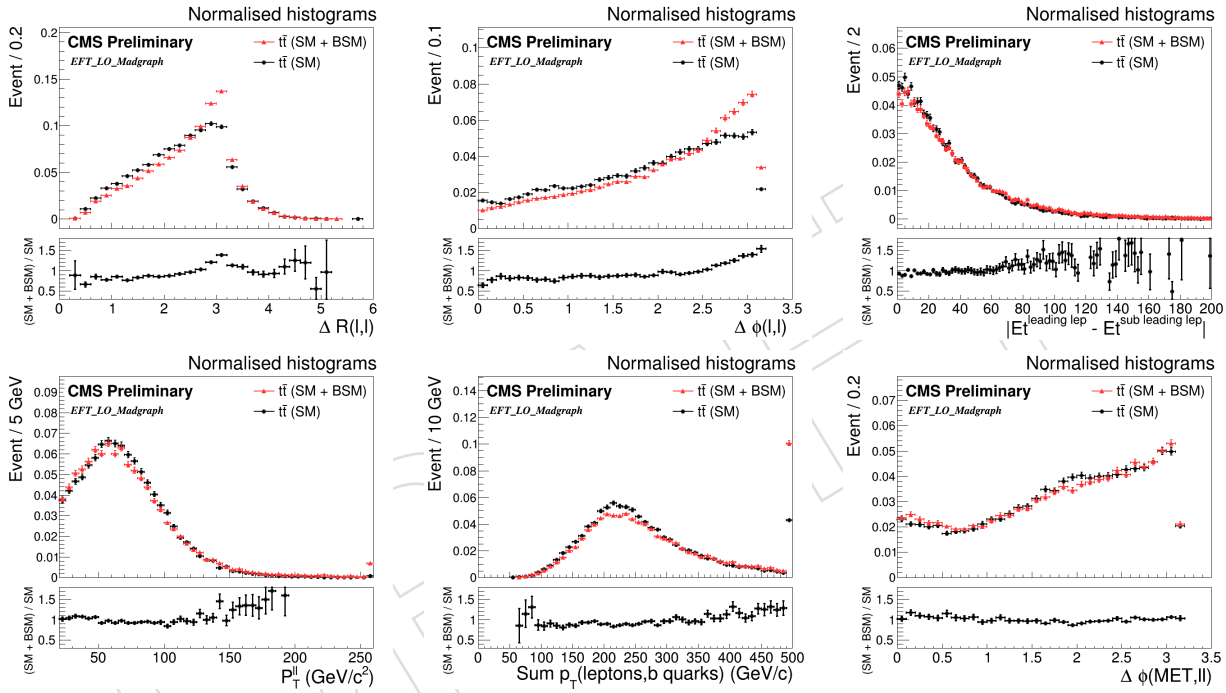

Figure 6: The distributions of some variables from operator O_G

.

4 Datasets and Monte Carlo Samples

Data and SM MC samples are discussed in [21].

4.1 Signal sample and cross section calculation

MadGraph5 is used to find the cross section of tW production in the presence of effective operators by issuing the following commands

```
 > import model TopEffTh
 > define p = p b b~
 > define all = ve vm vt ve~ vm~ vt~ e- mu- ta- e+ mu+ ta+
 > generate p p > t w- NP=2 QED=1 ,
 >(t > b w+ NP=0, w+ > all all), (w- > all all)
 > add process p p > t~ w+ NP=2 QED=1 ,
 > (t~ > b~ w-  QED=1 NP=0, w- > all all), (w+ > all all)
 > output
 > launch
```

For tW production via FCNC interactions we requested for full simulated samples. Sample names are sumarised in table 2. Public Feynrule files in which the FCNC effective Lagrangian is set are used [22]. The Feynrule files are passed to MadGraph 5 framework by means of the UFO model. Due to the fact that the kinematic distributions of the final state particles are independent of the strength of the FCNC couplings, signal samples are produced with an arbitrary assumption for C_{uG} and C_{cG}. The branching fraction of the top quark to W boson and b quark is assumed to be 100% at the generator level. Signal events from tau decays to electron or muon and neutrinos are also included in signal samples. Madgraph command for FCNC tW are

```
 > import model FCNC_Gluon
 > define all = ve vm vt ve~ vm~ vt~ e- mu- ta- e+ mu+ ta+
 > generate p p > t w- NP=1 ,
 > (t > b w+, w+ > all all), (w- > all all)
 > add process p p > t~ w+ NP=1 ,
 > (t~ > b~ w-, w- > all all), (w+ > all all)
```

sample
ST_tW_tcgFCNC_leptonDecays_Madgraph
ST_tW_tugFCNC_leptonDecays_Madgraph

Table 2: Signal MC samples (dataset=/*/RunIISummer16MiniAODv2*PUMoriond17_80X_mcRun2_asymptotic_2016_TrancheIV_v6*/MINIAODSIM)

5 Triggers

Trigger requierements are discussed in [21].

6 Event reconstruction and object identification

Object selection criteria are explained in [21].

Events are required to have at least two isolated leptons (electrons or muons) with opposite electric charge, and with an invariant mass above 20 GeV. The leading lepton should have a p_{T} above 25 GeV. For the same-flavor lepton channels, to suppress the Drell-Yan (Z/γ+jets) background, the invariant mass must not be within 15 GeV of the Z boson and a minimal value on the missing transverse momentum is applied, $p_{\mathrm{T}}^{\mathrm{miss}} > 60$ GeV.

The events are divided in the ee, eμ, and $\mu\mu$ channels according to the flavors of the two leptons with the highest p_{T} and are further categorised in different bins depending on the the number of jets ("n-jets") in the final state and the number of them which are b-tagged ("m-tags").

In order to probe $C_{\phi q}^{(3)}$, C_{tW}, C_{tG} and C_G coefficient, we use the following Categories:

- ee and $\mu\mu$ channels: (1-jet,1-tag), (2-jets,1-tag) and ($\geq$2-jets,2-tags)
- eμ channel: (1-jet,0-tag), (1-jet,1-tag), (2-jets,1-tag) and ($\geq$2-jets,2-tags)

For probing FCNC coefficients, C_{uG} and C_{cG}, events with exactly one b-jet are selected. Due to the fact that FCNC signal samples are generated at LO, number of signal events maybe affected by deviding signal regions due to the number of light jets. Therefore, we do not require any condition on the number of light jets.

- eμ, ee and $\mu\mu$ channels: (all-jet,1-tag)

7 Background predictions

SM background estimation procedures are explained in [21].

8 Signal extraction

The purpose of the analysis is to search for deviations to SM predictions in the $\mathrm{t\bar{t}}$ and tW production due to new physics, parametrised with the presence of the new effective couplings. All effective couplings introduced in section 1 can contribute to the tW production, while the O_{tG} operator also affects the $\mathrm{t\bar{t}}$ production. The operator $O_{\phi q}^{(3)}$ is similar to SM Wtb operator and leads to a re-scaling of the SM Wtb vertex. The O_{tW} and O_{tG} operators provide new interactions compared to the SM Wtb vertex and top-top-gluon (ttG) vertex. However, their effects have been investigated and found to be not easily distinguishable from SM tW and $\mathrm{t\bar{t}}$ processes through the various kinematic distributions of the final state particles. On the other hand, the presence of the O_{uG} and O_{cG} operators changes the initial state particle (see figure 1), and leads to different kinematic distribution for the final state particles, compared to the SM tW processes. For the FCNC operators, new physics effects can be more easily distinguished from SM processes.

In order to investigate the effect of the introduction of the new effective couplings, it is important to find suitable variables with high discrimination power between signal and the background. After the selection, the dominant background comes from the $\mathrm{t\bar{t}}$ production, with a contribution of about 90%. A multi-variate technique is used to seperate $\mathrm{t\bar{t}}$ events (the background) and tW events (considered as the signal) to search more efficiently for deviations from SM tW production in the presence of the $O_{\phi q}^{(3)}$, O_{tW} and O_{tG} effective couplings. In order to search for new physics due to the O_{uG} and O_{cG} effective couplings, a multi-variate technique is used to separate this time the SM backgrounds ($\mathrm{t\bar{t}}$ and tW events together) and the new physics signals.

The Multi Layer Perceptron (MLP) method is used in the analysis, a type of Neural Network (NN). Due to the variation of the background components in various signal regions, different input variables are employed in various bins of jets and b-jets multiplicities for separating SM tW events from other SM backgrounds. In order to search for $O_{\phi q}^{(3)}$, O_{tW} and O_{tG} operators, we use the MLPs found in [21].

For FCNC signal all regions are combined for MLP training. Input variables for the MLPs are shown in the table[1] 3. The following setting is used for MLP training,

```
> factory->BookMethod( TMVA::Types::kMLP, "MLP",
> "H:!V:NeuronType=sigmoid:VarTransform=N:NCycles=500:HiddenLayers=7:
> TestRate=10:EstimatorType=sigmoid" );
```

The distributionn of signal and background events are compared in figure 7. The ROC curve, epochs convergence and the correlations between the input variables are shown in figure 8. The MLP output for test and train samples are shown in figure 9.

Variable	Description	regions			
		1jets,0tag	1jets,1tag	2jets,1tag	FCNC
M_{ll}	invariant mass of dilepton system	$\surd$ (3)			$\surd$ (5)
$p_T^{\ell\ell}$	p_T of dilepton system	$\surd$ (1)		$\surd$ (4)	$\surd$ (3)
$\Delta p_T(\ell,\ell)$	$p_T^{\text{leading lepton}}$ - $p_T^{\text{sub-leading lepton}}$	$\surd$ (2)			$\surd$ (4)
$p_T^{\text{leading lepton}}$	p_T of leading lepton	$\surd$ (4)		$\surd$ (2)	$\surd$ (1)
Centrality(ℓ^{leading} jet$^{\text{leading}}$)	scalar sum of p_T of the leading lepton and leading jet,over total energy of selected objects	$\surd$ (7)			$\surd$ (9)
Centrality($\ell\ell$)	scalar sum of p_T of the leading and sub-leading leptons,over total energy of selected objects	$\surd$ (6)			$\surd$ (7)
$\Delta\phi$($\ell\ell$,jet$^{\text{leading}}$)	$\Delta\phi$ between dilepton system and leading jet	$\surd$ (5)	$\surd$ (3)	$\surd$ (5)	
p_T($\ell\ell$,jet$^{\text{leading}}$)	p_T of dilepton and leading jet system		$\surd$ (1)		$\surd$ (6)
p_T(ℓ^{leading} ,jet$^{\text{leading}}$)	p_T of leading lepton and leading jet system		$\surd$(2)		
Centrality($\ell\ell$ jet$^{\text{leading}}$)	scalar sum of p_T of the dilepton system and leading jet,over total energy of selected objects		$\surd$ (4)		
ΔR(ℓ,ℓ)	ΔR between leading and sub-leading leptons		$\surd$ (6)		
ΔR(ℓ^{leading},jet$^{\text{leading}}$)	ΔR between leading lepton and leading jet		$\surd$ (5)		
M(ℓ^{leading}, jet$^{\text{sub-leading}}$)	invariant mass of leading lepton and leading jet			$\surd$ (1)	
M(jet$^{\text{leading}}$, jet$^{\text{sub-leading}}$)	invariant mass of leading jet and sub-leading jet			$\surd$ (3)	
ΔR(ℓ^{leading},jet$^{\text{sub-leading}}$)	ΔR between leading lepton and sub-leading jet			$\surd$ (6)	
ΔR($\ell\ell$,jet$^{\text{leading}}$)	ΔR between dilepton system and leading jet			$\surd$ (7)	$\surd$ (8)
Δp_T($\ell^{\text{sub-leading}}$, jet$^{\text{sub-leading}}$)	$p_T^{\text{sub-leading lepton}}$ - $p_T^{\text{sub-leading jet}}$			$\surd$ (8)	
M($\ell^{\text{sub-leading}}$, jet$^{\text{leading}}$)	invariant mass of sub-leading lepton and leading jet				$\surd$ (2)

Table 3: Input variables for the MLPs used in the analysis in various bins of jets and b-jets multiplicities. The symbol $\surd$ represents the variables used for each particular MLP and the rank of variables are shown for each region. Input variables used in MVA training for FCNC signal are shown in the last culumn.

[1] Loose jets are jets with p_T range between 20 GeV and 30 GeV and $|\eta|$ <2.4

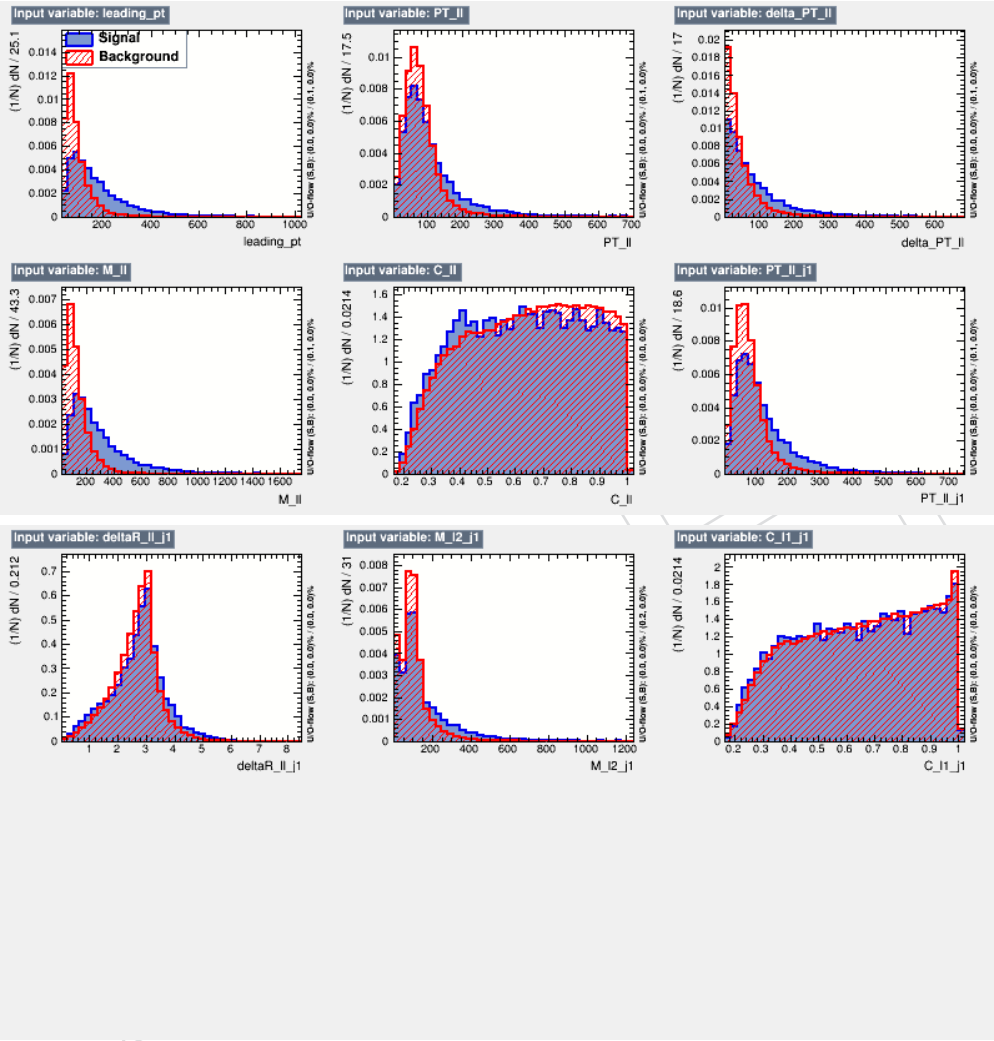

Figure 7: FCNC: MLP input variable distributions in all regions. Signal distributions are drawn in blue and the background distributions in red.

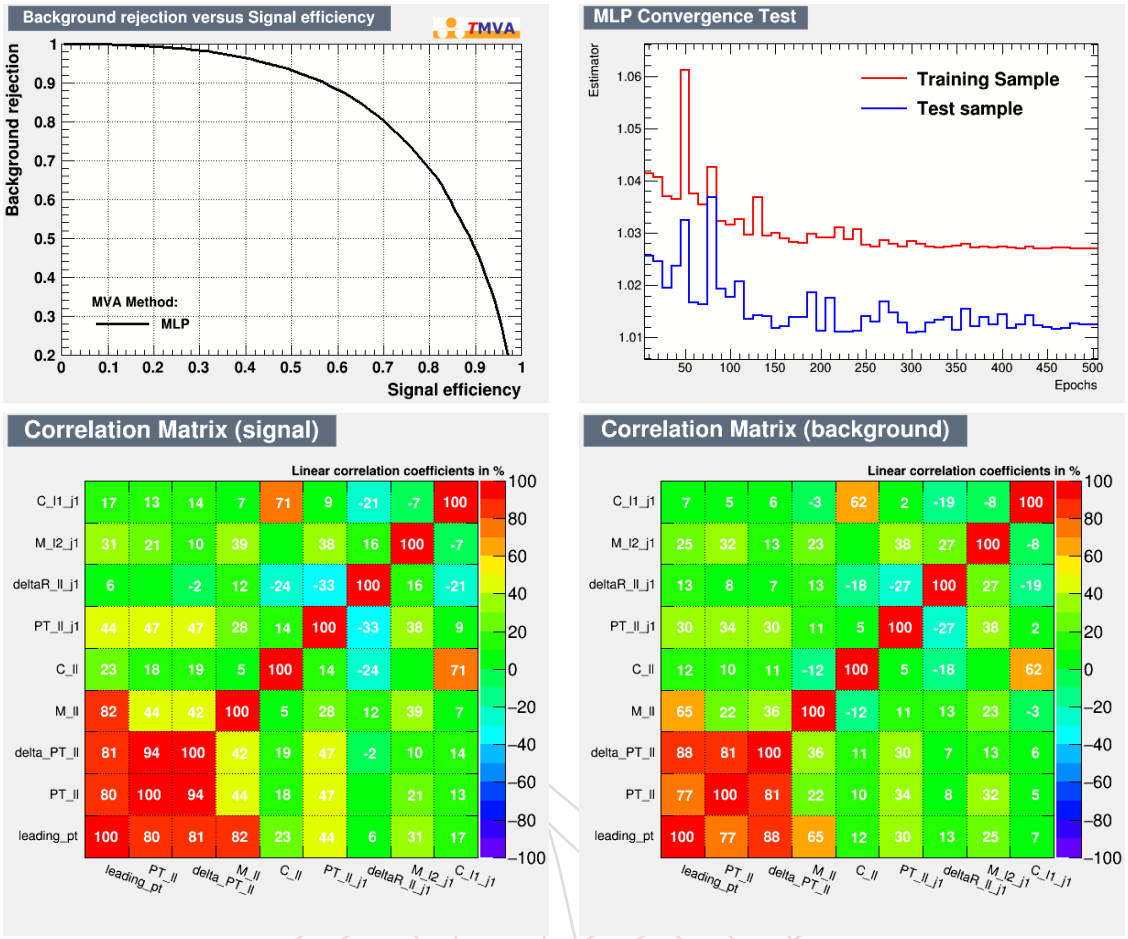

Figure 8: FCNC: The ROC curve and epochs convergence (top) and the correlation matix for signal (bottom left) and background (bottom right).

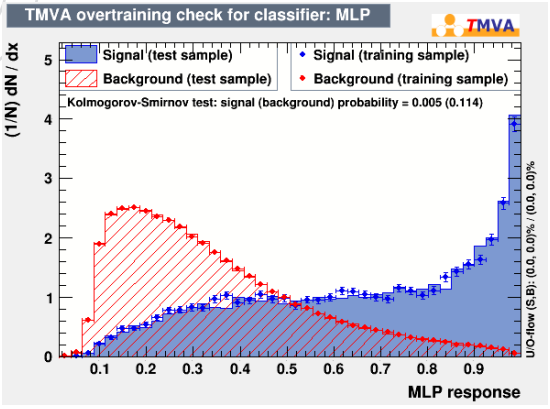

Figure 9: FCNC: The MLP response.

8.1 Data/MC comparison for MVA input variables

The FCNC signal, data and MC comparison for MVA input variables are shown in 10, 11, and 12 for 1tag region. Find data and MC comparison plots for MLP output used for probing $O_{\phi q}^{(3)}$, O_{tW} and O_{tG} operators in [21].

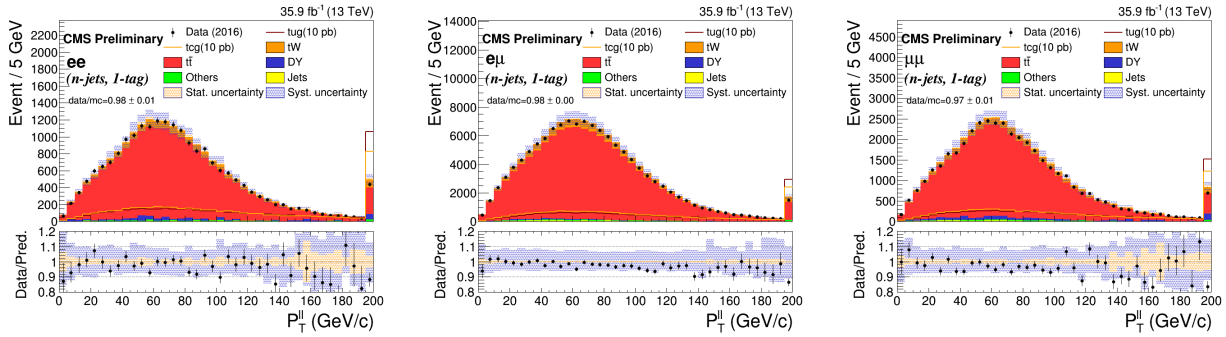

Figure 10: The distributions of variables used for MVA input for FCNC study for ee (left), $e\mu$ (middle) and $\mu\mu$ (right) channels for 1 b-jet region.

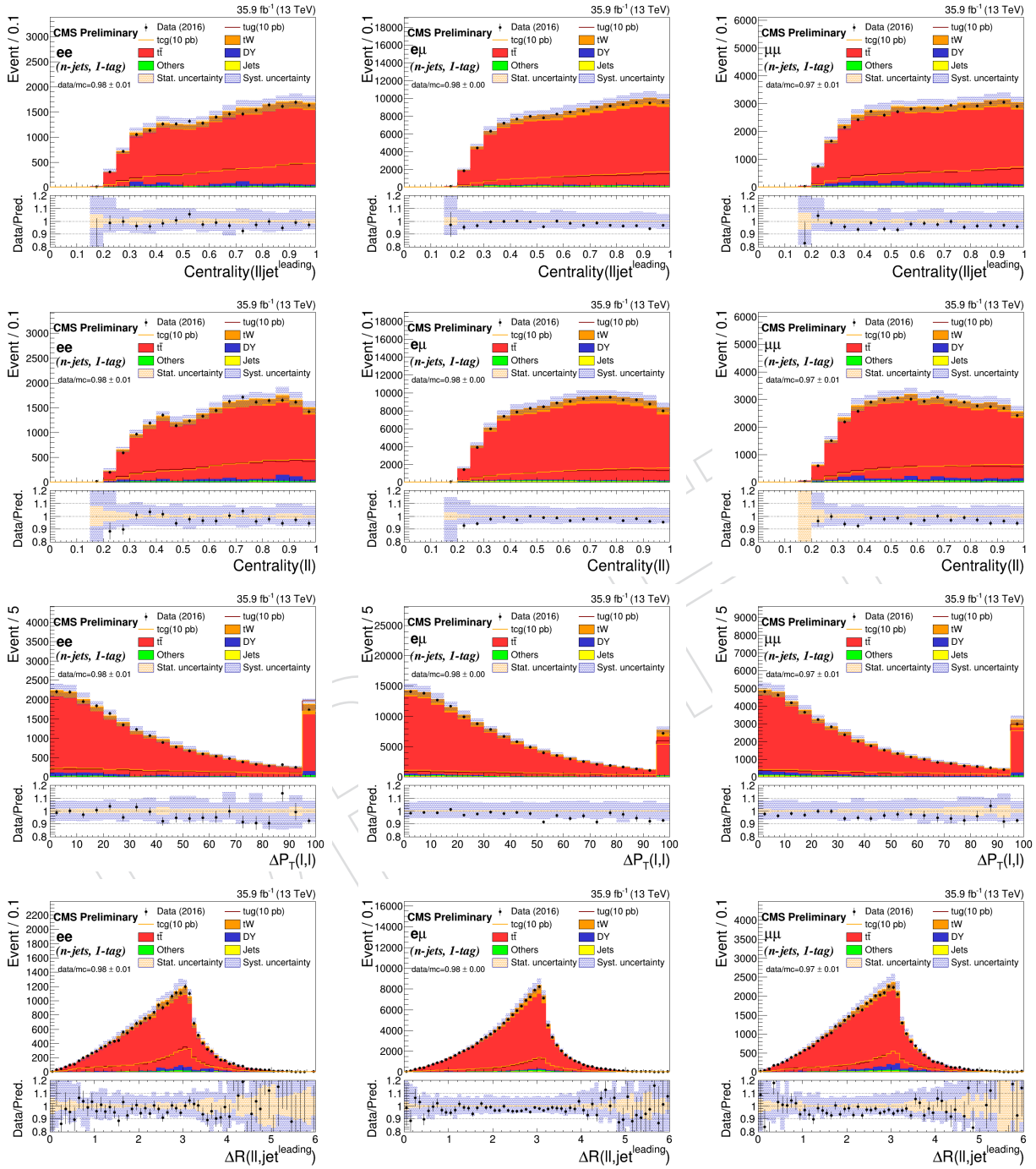

Figure 11: The distributions of variables used for MVA input for FCNC study for ee (left), $e\mu$ (middle) and $\mu\mu$ (right) channels for 1 b-jet region.

The O_G operator affects only the $t\bar{t}$ production. It was shown in Ref. [4] and checked in this analysis that the $t\bar{t}$ transverse momentum distribution is sensitive to the triple field strength operator. Due to the fact that the kinematic distributions of final state particles show less discrimination power compared to top transverse momentum distribution, we avoid training a dedicated MVA and use the total number of events in data and prediction in various (n-jets,m-tags) categories to constrain the C_G effective coupling.

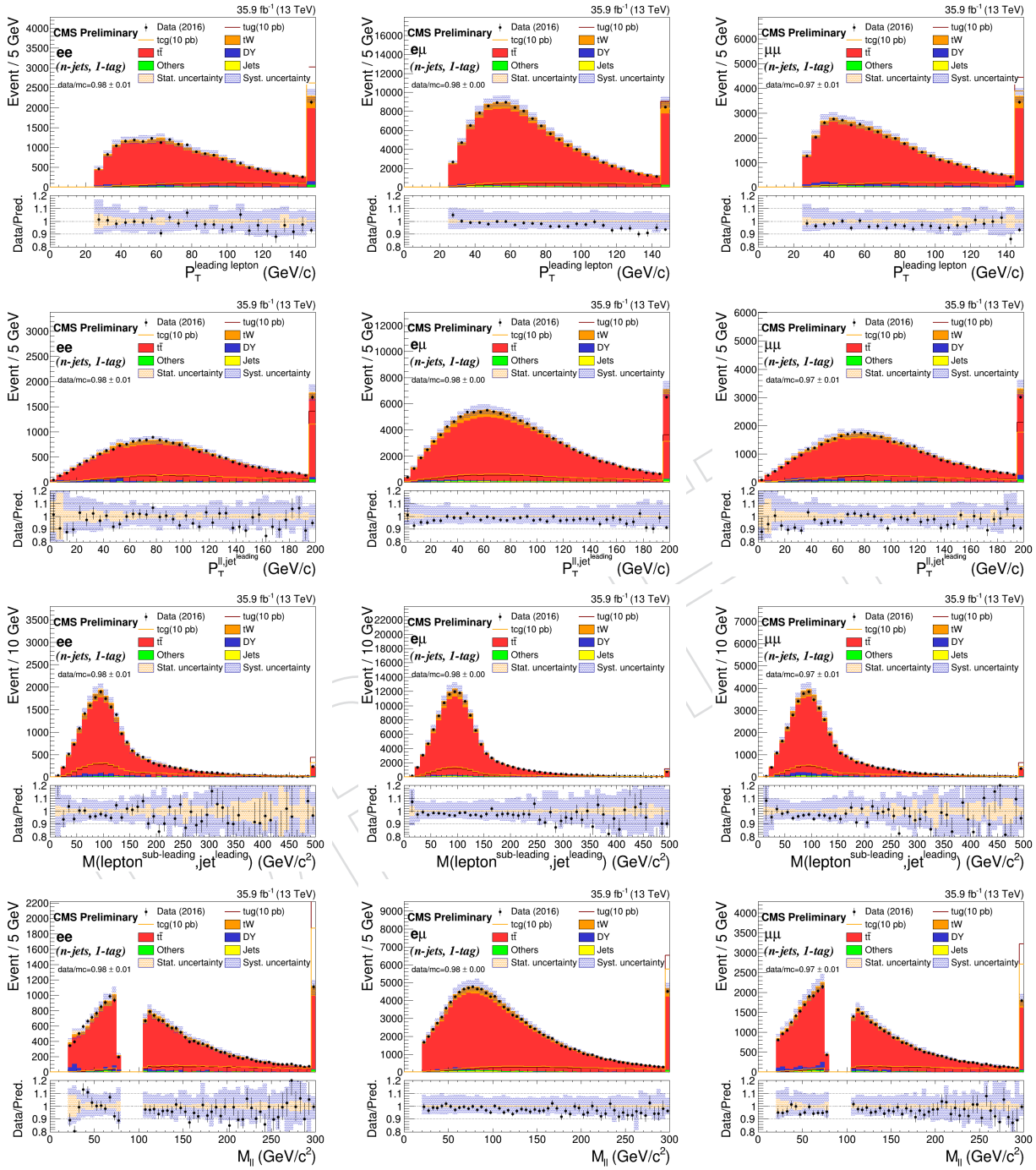

Figure 12: The distributions of variables used for MVA input for FCNC study for ee (left), $e\mu$ (middle) and $\mu\mu$ (right) channels for 1 b-jet region.

9 Systematic uncertainties

This analysis depends on both the normalization and shape of the background and signal expectations. We consider all sources of systematic uncertainties that are discussed in the tW measurement analysis (see [21] for full list of the systematic sources).

Due to the observed difference between the $t\bar{t}$ kinematic distribution with and without C_G

In addition, we consider following sources of uncertainties on FCNC signal. ***Parton Distribution Functions uncertainty:*** The magnitude of the uncertainties related to the parton distribution functions and the variation of the strong coupling constant for FCNC tW simulated signal processes is obtained using the replicas of the NNPDF 3.0 set. Each event is weighted with respect to the LHE weights provided for each replicas of the NNPDF 3.0 set and final NN distribution is found. One sigma UP/DOWN uncertainty from the distribution of the NN output due to the various PDF set with respect to the nominal set is assigned as PDF error. ***QCD scale uncertainty:*** This uncertainty is estimated by varying the renormalization and the factorization scales for FCNC tW simulated signal, used during the MC generation of the sample by a factor 0.5 and or 2. Each event is weighted with respect to the LHE weights provided for renomalization and factorization scale variation. The largest deviation from the nominal value is taken as QCD scale error. ***Parton shower Q scale uncertainty:*** The scales of the initial (ISR) and final (FSR) state shower are varied up and down by a factor of two FCNC tW simulated signal samples. MC samples used to estimate the parton shower Q scale uncertainties are sumarrised in table 4.

sample
ST_tW_tcgFCNC_scaledown_leptonDecays_Madgraph
ST_tW_tcgFCNC_scaleup_leptonDecays_Madgraph
ST_tW_tugFCNC_scaledown_leptonDecays_Madgraph
ST_tW_tugFCNC_scaleup_leptonDecays_Madgraph

Table 4: FCNC systematic samples (dataset=/*/RunIISummer16MiniAODv2*PUMoriond17_80X_mcRun2_asymptotic_2016_TrancheIV_v6*/MINIAODSIM)

10 Results

The expected number of events from the tW and the $t\bar{t}$ production, as well as from the sum of all background contributions mentioned above are reported in table 5 for the ee, eμ and $\mu\mu$ channels and for various (njet, nbjet) categories. In figure 13, the data in the 10 search regions are shown in comparison with the summed predictions for the SM backgrounds.

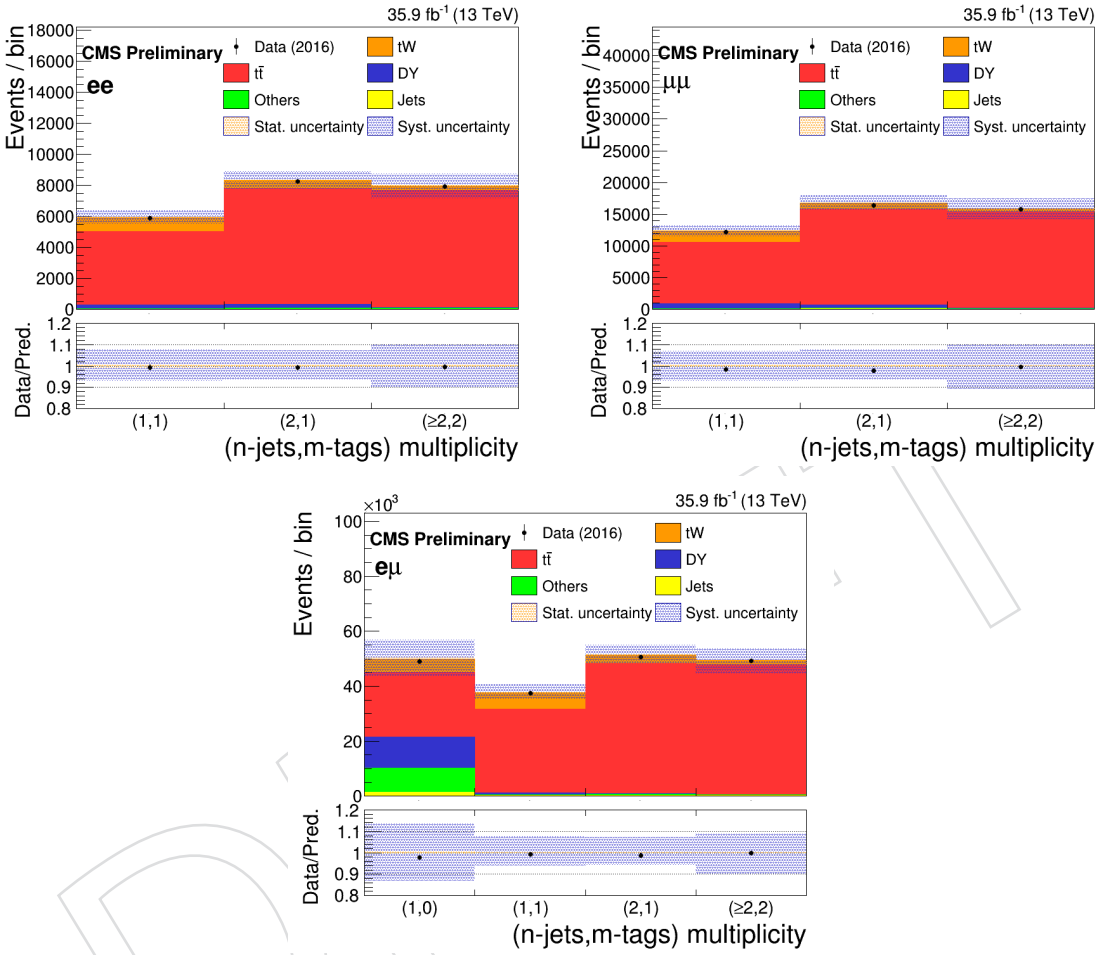

Figure 13: The observed numbers of events and SM background predictions in the search regions of the analysis for ee channel (top left), $\mu\mu$ channel (top right) and eμ channel (bottom). The blue hatched bands correspond to the sum of statistical and systematic uncertainties in the event yield for the sum of signal and background predictions. The ratios of data to the sum of the predicted yields are shown at the bottom of each plot. Here, an additional solid yellow band represents the contribution from the statistical uncertainty in the MC simulation.

10.1 Limit setting procedure

For those operators which interfere with the SM, C_G-C_{tG}-$C_{\phi q}$-C_{tW}, normalization of the $t\bar{t}$ or tW process is directly extracted from a fit to data. Normalization of the signal (tW/ $t\bar{t}$) is parametrized as

$$\sigma = \sigma_{SM} + C_i\sigma_i^{(1)} + C_i^2\sigma_i^{(2)}\,, \tag{19}$$

in which σ_{SM}, $\sigma_i^{(1)}$ and $\sigma_i^{(2)}$ are fixed parameters (see table 1) and C is the parameter of interest in

Channel	(njet,nbjet)	Data	MC simulations		
			tW	$t\bar{t}$	Total backgrounds
ee	(1jet, 1bjet)	5902±76(stat.)	884±8(stat.)	4741±15(stat.)	5936±470(stat.+syst.)
	(2jet, 1bjet)	8266±90(stat.)	518±6(stat.)	7479±19(stat.)	8331±597(stat.+syst.)
	(≥2jet, 2bjet)	7945±89(stat.)	267±4(stat.)	7561±18(stat.)	7973±819(stat.+syst.)
eμ	(1jet, 0bjet)	48973±221(stat.)	4835±20(stat.)	23557±35(stat.)	50038±6931(stat.+syst.)
	(1jet , 1bjet)	37370±193(stat.)	6048±22(stat.)	30436±38(stat.)	37673±2984(stat.+syst.)
	(2jet, 1bjet)	50725±225(stat.)	3117±16(stat.)	47206±48(stat.)	51382±3714(stat.+syst.)
	(≥2jet, 2bjet)	49262±221(stat.)	1450±10(stat.)	47310±46(stat.)	49391±5010(stat.+syst.)
$\mu\mu$	(1jet, 1bjet)	12178±110(stat.)	1738±12(stat.)	9700±21(stat.)	12366±879(stat.+syst.)
	(2jet, 1bjet)	16395±128(stat.)	989±9(stat.)	14987±27(stat.)	16751±1276(stat.+syst.)
	(≥2jet, 2bjet)	15838±125(stat.)	508±6(stat.)	15136±26(stat.)	15889±1714(stat.+syst.)

Table 5: Numbers of observed events in data, expected events from tW and $t\bar{t}$ production, and the total background contribution (tW and $t\bar{t}$ production, Drell-Yan and diboson processes, W+jets and multijets backgrounds) after all selections for the ee, eμ and $\mu\mu$ channels and for various (njet, nbjet) categories.

the fit. In order to evaluate the effect of the uncertainties on σ_{SM}, $\sigma_i^{(1)}$ and $\sigma_i^{(2)}$, fit is performed when these parameters are varied $\pm\sigma$ because of the Q scale uncertainties. All three terms are considered fully correlated for Q-scale variation based on the recommendation from theorists. In addition, uncertainties due to PDF is considered. Results of the mentioned variations are only shown for observed limits for comparison to the nominal results. In table 6, nominal values for $\sigma_i^{(1)}$ and $\sigma_i^{(2)}$ are shown together with errors.

Table 6: Cross sections for $t\bar{t}$ and tW production [in pb] for the various effective couplings for Λ = 1 TeV together with Q-scale errors.

Channel	σ_{SM} (scale unc.) (PDF+alphaS unc.)
$t\bar{t}$	831.76 (+19.77, -29.20), (+35.06, -35.06)
tW	71.7 (+1.80, -1.80), (+3.40 -3.40)

Channel	$\sigma_i^{(1)}$ (scale unc.)
$t\bar{t}$	202.83 C_{tG} (+24.54,-26.98) , 31.9 C_G (+8.1,-6.9)
tW	8.844 $C_{\phi q}$ (+0,-0) ,-5.65 C_{tW} (+0.08317,-0.061846) , 4.223 C_{tG} (+0.0294,-0.0398)

Channel	$\sigma_i^{(2)}$ (scale unc.)
$t\bar{t}$	23.545 C_{tG}^2 (+0,-0) , 102.3 C_G^2 (+22.7,-15.3)
tW	0.275 $C_{\phi q}^2$ (+0,-0) , 1.18 C_{tW}^2 (+0.0283,-0.0257) , 1.322 C_{tG}^2 (+0.0558,-0.0335) , 21.209 C_{uG}^2 (+1.485,-1.273) , 5.804 C_{cG}^2 (+0.255,-0.250)

Scale uncertainties are calculated at NLO for C_{tG}, $C_{\phi q}$ and C_{tW} and LO for C_G, C_{uG} and C_{cG}.

10.2 Exclusion limits on C_G effective coupling

It was discussed in section 1 that the operator O_G operator only contributes to $t\bar{t}$ production process. It was shown in figure 6 that the shapes of some variables are affected in the presence of the O_G operator. On the other hand, the effect is not big enough to be observed experimentaly in ttbar kinematic distributions as a shape effect. Therefore, the fit is performed simultaneously on the observed event yield in (1-jet,1-tag), (2-jet,1-tag) and (≥2-jet,2-tag) categories for ee, eμ and $\mu\mu$ channels. In addition, the (1-jet,0-tag) category is included only for the eμ channel. The results for individual channels and combined channels are listed in Table 7. The results of the likelihood scans of the C_G coupling is shown in Fig. 14.

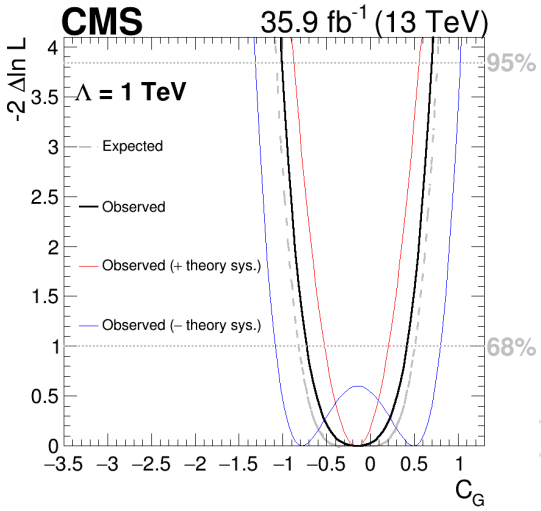

Figure 14: Likelihood scan of C_G effective coupling.

	Regions	best fit exp./obs.	68% exp./obs.limit	95% exp./obs.limit
C_G	$e\mu$ yield (1j1t)	0.00 / -0.18	[-0.93 to 0.62]/[-0.88 to 0.57]	[-1.24 to 0.93]/[-1.20 to 0.89]
	$e\mu$ yield (1j1t), (2j1t), ($\geq$2j,2t)	0.00 / -0.14	[-0.82 to 0.51]/[-0.73 to 0.42]	[-1.08 to 0.77]/[-1.01 to 0.70]
	$e\mu$ yield (1j0t), (1j1t), (2j1t), ($\geq$2j,2t)	0.00 / -0.18	[-0.82 to 0.51]/[-0.73 to 0.42]	[-1.08 to 0.77]/[-1.01 to 0.70]
	ee yield (1j1t), (2j1t), ($\geq$2j,2t)	0.00 / -0.14	[-0.90 to 0.59]/[-0.82 to 0.51]	[-1.20 to 0.88]/[-1.14 to 0.83]
	$\mu\mu$ yield (1j1t), (2j1t), ($\geq$2j,2t)	0.00 / -0.14	[-0.88 to 0.57]/[-0.75 to 0.44]	[-1.16 to 0.85]/[-1.06 to 0.75]
	Combined	0.00 / -0.18	[-0.82 to 0.51]/[-0.73 to 0.42]	[-1.07 to 0.76]/[-1.01 to 0.70]

Table 7: Summary of allowed 68% CL and 95% CL intervals on C_G effective coupling obtained in ee, $e\mu$, $\mu\mu$ and combined channels ($\Lambda = 1TeV$).

10.3 Exclusion limits on C_{tG}, $C_{\phi q}$ and C_{tW} effective couplings

The deviation from the SM tW production from the interference terms between the SM and the O_{tG}, $O_{\phi q}$ and O_{tW} operators is of the order of $\frac{1}{\Lambda^2}$. It is assumed that the new physics scale, Λ, is larger than the scale we probe. Therefore, $\frac{1}{\Lambda^4}$ contributions, pure new physics term, would be small compared to the contribution from the interference term. Following the strategy described in section 1, in the likelihood fit, the signal probability density function (pdf) originates from the sum of the SM term, the interference term and the pure new physics term is assumed to be the same as the SM tW (or $t\bar{t}$ for O_{tG}) pdf.

In order to set limits on the effective couplings C_{tG}, $C_{\phi q}$ and C_{tW}, we utilize the MLP output distributions for both data and MC expectation in the (1jet,1b-jet) and (2jet,1b-jet) regions and event yield in the ($\geq$2jet,2b-jet) region for all the three channels. The MLP is trained to separate tW from $t\bar{t}$ events as was discussed in section 8. The inclusion of the ($\geq$2jet,2b-jet) and (2jet,1b-jet) regions helps to constrain the normalization and systematic uncertainties of the $t\bar{t}$ background. In addition, the (1jet,0b-jet) region is included for the eμ channel to increase signal sensitivity while this region is not used in *ee* and $\mu\mu$ channels because of the huge DY contamination. Comparison between observed data and the SM background prediction for the MLP output shape in various jet-bjet regions are shown in figure 15.

Three Wilson coefficients sensitive to new physics contribution in top quark interactions, as defined in equations 5-7 are tested in observed data. The results of the likelihood scans of the Wilson coefficients on the full 13 TeV dataset are shown in figure 16 for combined channels. In another CMS analysis [23], limits on C_{tG} is found using the differential distribution of $\Delta\phi(\ell\ell)$. In order to remove overlap (FIXME: is this separation necessary?), we do not use regions with $>= 2$ jets. Therefore, independent limits are found after removing regions with $>= 2$ jets. The results for individual channels and combined channels are listed in table 8.

		best fit exp./obs.	68% exp./obs.limit	95% exp./obs.limit
$C_{\phi q}$	eμ NN output for (1j1t)	0.00 / -0.90	[-2.58 to 1.99]/[-4.05 to 1.42]	[-5.56 to 3.81]/[-8.30 to 3.23]
	eμ NN output for (1j1t+2j1t) + yields($\geq$2j,2t)	0.00 / -0.73	[-1.36 to 1.14]/[-2.17 to 0.63]	[-2.64 to 2.18]/[-3.75 to 1.68]
	eμ NN output for (1j0t+1j1t+2j1t) + yields($\geq$2j,2t)	0.00 / -0.70	[-1.34 to 1.12]/[-2.16 to 0.59]	[-2.57 to 2.15]/[-3.74 to 1.61]
	ee NN output for (1j1t+2j1t) + yields($\geq$2j,2t)	0.00 / 1.12	[-2.53 to 1.74]/[-1.18 to 2.89]	[-6.40 to 3.27]/[-4.03 to 4.37]
	$\mu\mu$ NN output for (1j1t+2j1t) + yields($\geq$2j,2t)	0.00 / 1.13	[-2.20 to 1.92]/[-0.87 to 2.86]	[-4.68 to 3.66]/[-3.58 to 4.46]
	Combined	0.00 / -1.52	[-1.05 to 0.88]/[-2.71 to -0.33]	[-2.04 to 1.63]/[-3.82 to 0.63]
C_{tW}	eμ NN output for (1j1t)	0.00 / 2.17	[-2.25 to 7.04]/[-1.72 to 6.51]	[-3.75 to 8.54]/[-3.30 to 8.09]
	eμ NN output for (1j1t+2j1t)+yields($\geq$2j,2t)	0.00 / 3.08	[-1.42 to 6.21]/[-0.86 to 5.65]	[-2.42 to 7.21]/[-1.97 to 6.76]
	eμ NN output for (1j0t+1j1t+2j1t)+yields($\geq$2j,2t)	0.00 / 1.64	[-1.40 to 6.19]/[-0.80 to 5.59]	[-2.39 to 7.18]/[-1.89 to 6.68]
	ee NN output for (1j1t+2j1t)+yields($\geq$2j,2t)	0.00 / 6.18	[-2.02 to 6.81]/[-3.02 to 7.81]	[-3.33 to 8.12]/[-4.16 to 8.95]
	$\mu\mu$ NN output for (1j1t+2j1t)+yields($\geq$2j,2t)	0.00 / -1.40	[-2.18 to 6.97]/[-3.00 to 7.79]	[-3.63 to 8.42]/[-4.23 to 9.01]
	Combined	0.00 / 2.38	[-1.14 to 5.93]/[0.22 to 4.57]	[-1.91 to 6.70]/[-0.96 to 5.74]
C_{tG}	eμ NN output for (1j1t)	0.00 / 0.01	[-0.26 to 0.20]/[-0.24 to 0.21]	[-0.52 to 0.39]/[-0.46 to 0.39]
	eμ NN output for (1j1t+2j1t)+yields($\geq$2j,2t)	0.00 / -0.05	[-0.18 to 0.15]/[-0.20 to 0.12]	[-0.35 to 0.30]/[-0.35 to 0.27]
	eμ NN output for (1j0t+1j1t+2j1t)+yields($\geq$2j,2t)	0.00 / -0.03	[-0.17 to 0.15]/[-0.19 to 0.11]	[-0.34 to 0.29]/[-0.34 to 0.27]
	ee NN output for (1j1t+2j1t)+yields($\geq$2j,2t)	0.00 / -0.19	[-0.22 to 0.21]/[-0.40 to 0.02]	[-0.44 to 0.41]/[-0.65 to 0.22]
	$\mu\mu$ NN output for (1j1t+2j1t)+yields($\geq$2j,2t)	0.00 / -0.15	[-0.19 to 0.18]/[-0.34 to 0.02]	[-0.40 to 0.35]/[-0.53 to 0.19]
	Combined	0.00 / -0.13	[-0.15 to 0.14]/[-0.27 to 0.02]	[-0.30 to 0.28]/[-0.41 to 0.17]
C_{tG}	eμ NN output for (1j0t+1j1t)	0.00 / -0.01	[-0.25 to 0.19]/[-0.24 to 0.21]	[-0.52 to 0.37]/[-0.45 to 0.40]
	ee NN output for (1j1t)	0.00 / -0.03	[-0.31 to 0.27]/[-0.31 to 0.23]	[-0.58 to 0.52]/[-0.61 to 0.48]
	$\mu\mu$ NN output for (1j1t)	0.00 / -0.03	[-0.26 to 0.25]/[-0.29 to 0.21]	[-0.51 to 0.49]/[-0.54 to 0.44]
	Combined	0.00 / 0.03	[-0.21 to 0.18]/[-0.16 to 0.21]	[-0.42 to 0.35]/[-0.35 to 0.38]

Table 8: Summary of allowed 68% CL and 95% CL intervals on C_{tG}, $C_{\phi q}$ and C_{tW} effective couplings obtained in *ee*, eμ, $\mu\mu$ and combined channels ($\Lambda = 1TeV$).

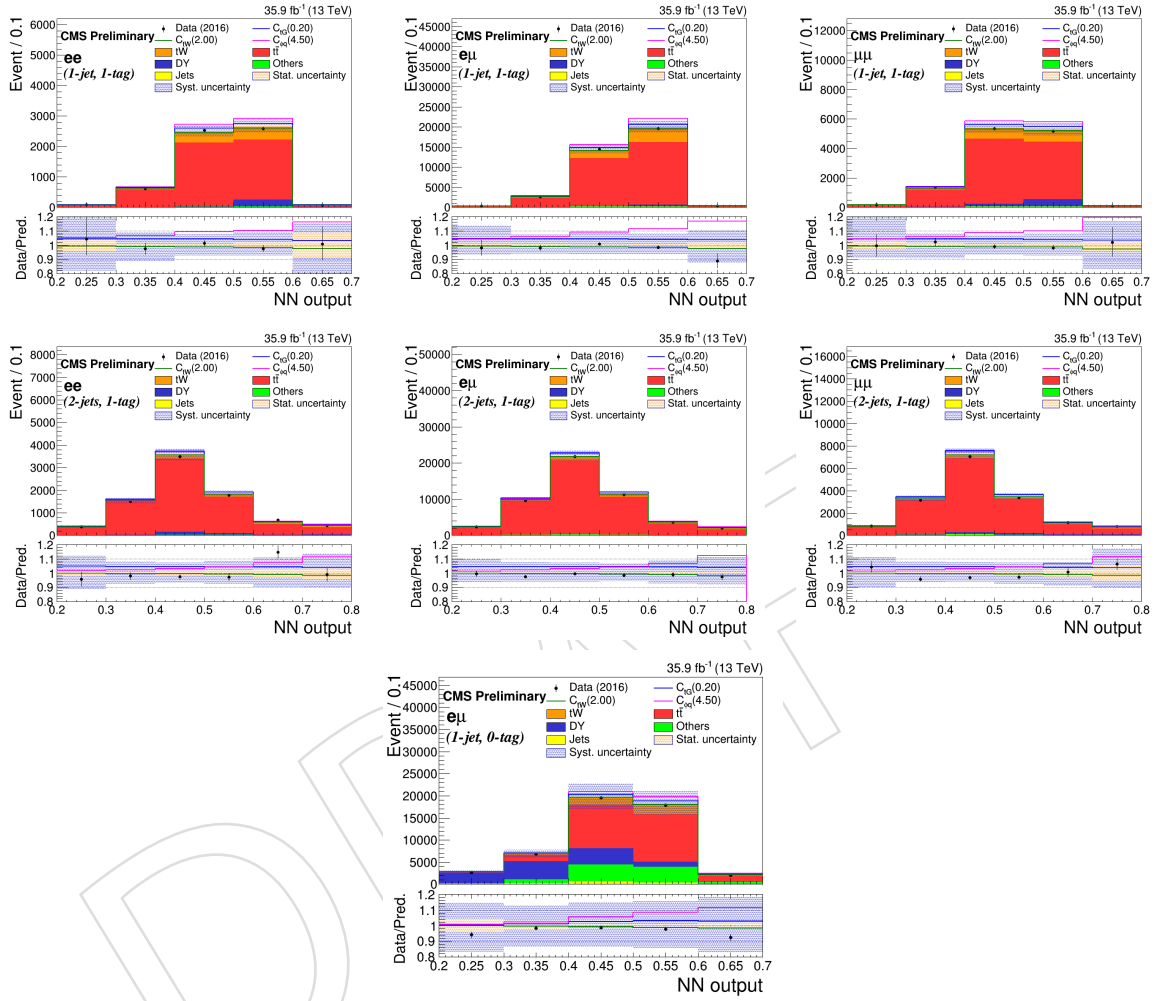

Figure 15: The MLP distribution of data and MC in different regions: (1jet,1b-jet) (top row), (2jet,1b-jet) (middle row) and (1jet,0b-jet) (bottom row) used in limit setting for ee channel (left column) $e\mu$ channel (middle column) $\mu\mu$ channel (right column). The blue hatched bands correspond to the sum of statistical and systematic uncertainties in the event yield for the sum of signal and background predictions. The ratios of data to the sum of the predicted yields are shown at the bottom of each plot. Here, an additional solid yellow band represents the contribution from the statistical uncertainty in the MC simulation.

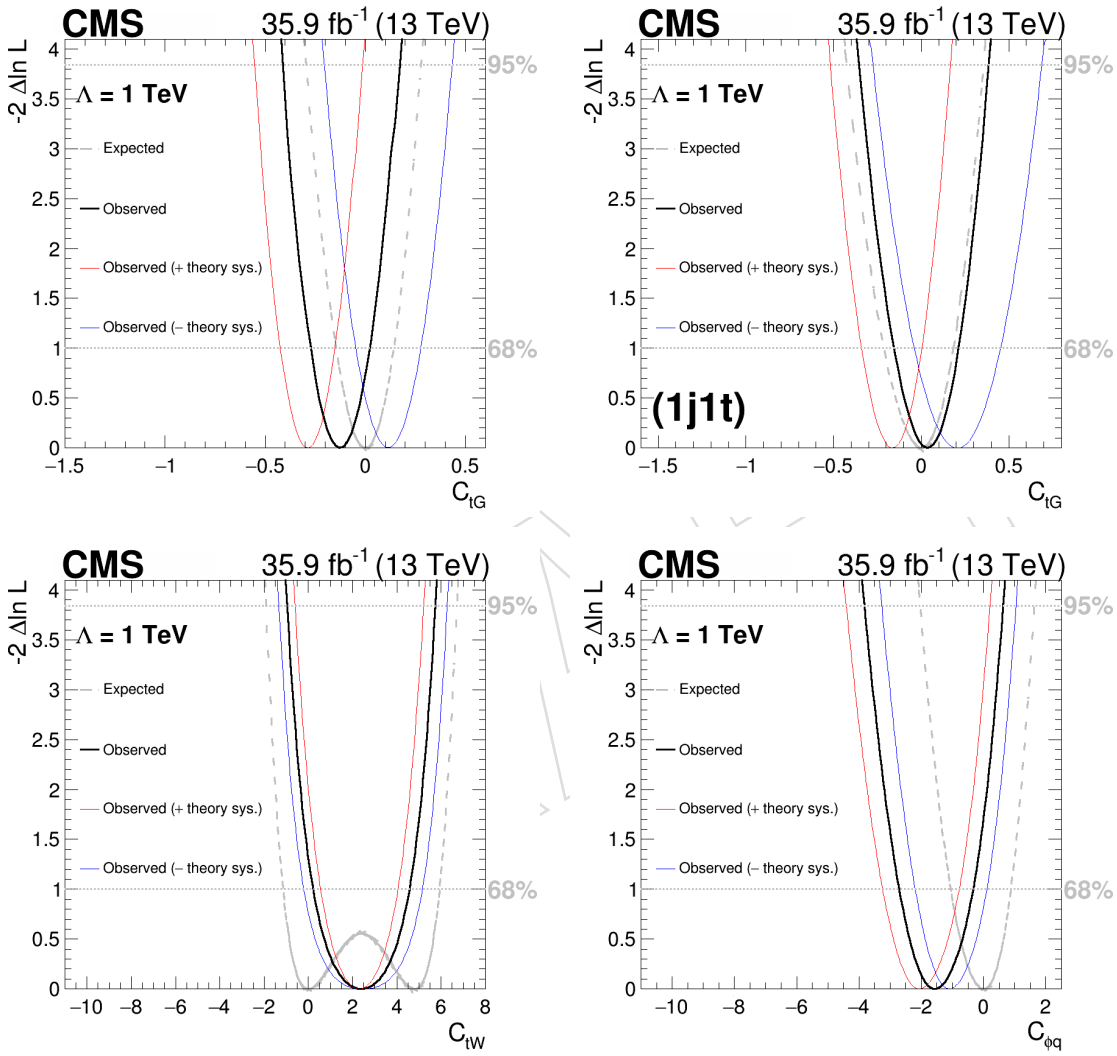

Figure 16: Likelihood scans of C_{tG}, $C_{\phi q}$ and C_{tW} effective couplings.

10.4 Exclusion limits on C_{uG} and C_{cG} effective couplings

Since the tW production via FCNC interactions doesn't interference with the SM (with the assumption of $|V_{td}| = |V_{ts}| = 0$), independent pdf for signal is considered to set upper bound on related Wilson coefficients. The comparison of the MLP output for the data, SM background and signal (tW events via FCNC interactions) in various (jet,b-jet) multiplicity are shown in figure 17. All regions introduced in previous section are included in limit setting procedure. The MLP is trained to separate FCNC tW events from SM tW and $t\bar{t}$ events as discussed in section 8 The results of the likelihood scans of the Wilson coefficients on the full 13 TeV dataset are shown in figure 18 for combined channels. The observed and median expected 95% CL upper limits on the $\sigma(pp\rightarrow tW)\times B(W\rightarrow \ell\nu)^2$ for FCNC signals are given for combined channel in table 10. These individual limits can be used to calculate the upper limits on the Wilson coefficients C_{uG}, C_{cG}, and on the branching fractions B(t $\rightarrow$ ug) and B(t $\rightarrow$ cg).

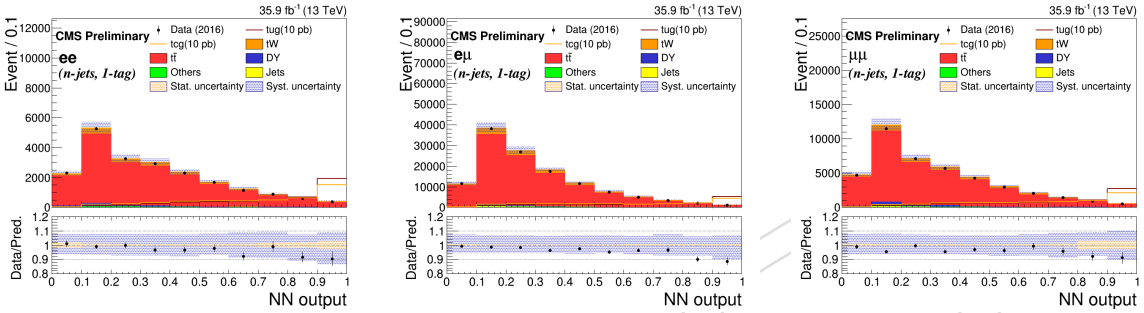

Figure 17: The MLP distribution of data, MC and FCNC signals in 1b-jet region used in limit setting for *ee* channel (left column) $e\mu$ channel (middle column) $\mu\mu$ channel (right column). The blue hatched bands correspond to the sum of statistical and systematic uncertainties in the event yield for the sum of signal and background predictions. The ratios of data to the sum of the predicted yields are shown at the bottom of each plot. Here, an additional solid yellow band represents the contribution from the statistical uncertainty in the MC simulation.

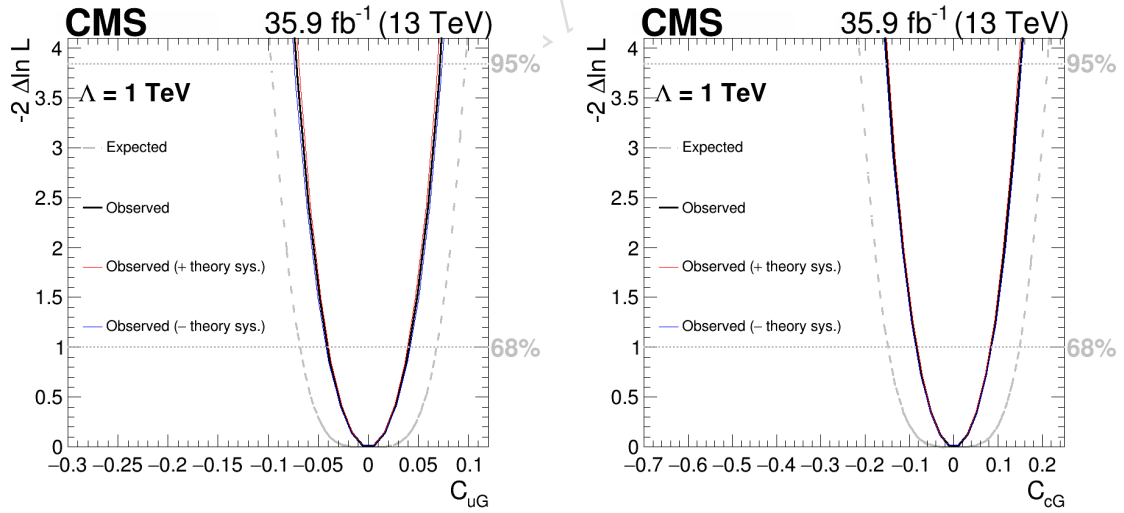

Figure 18: Likelihood scans of C_{uG} and C_{cG} effective couplings.

The expected and observed upper limits on the Wilson coefficients obtained from the combination of all channels and signal regions are visualized in Figure 19.

		best fit exp./obs.	68% exp./obs.limit	95% exp./obs.limit
C_{uG}	eμ NN output for (1t)	0.00 / -0.01	[-0.08 to 0.08]/[-0.05 to 0.05]	[-0.12 to 0.12]/[-0.09 to 0.09]
	ee NN output for (1t)	0.00 / -0.01	[-0.09 to 0.09]/[-0.07 to 0.07]	[-0.14 to 0.14]/[-0.12 to 0.12]
	$\mu\mu$ NN output for (1t)	0.00 / -0.01	[-0.09 to 0.09]/[-0.05 to 0.05]	[-0.12 to 0.12]/[-0.09 to 0.09]
	Combined	0.00 / -0.01	[-0.07 to 0.07]/[-0.04 to 0.04]	[-0.10 to 0.10]/[-0.07 to 0.07]
C_{cG}	eμ NN output for (1t)	0.00 / -0.01	[-0.18 to 0.18]/[-0.11 to 0.11]	[-0.26 to 0.26]/[-0.19 to 0.19]
	ee NN output for (1t)	0.00 / -0.01	[-0.20 to 0.20]/[-0.15 to 0.15]	[-0.30 to 0.30]/[-0.25 to 0.25]
	$\mu\mu$ NN output for (1t)	0.00 / -0.01	[-0.19 to 0.19]/[-0.12 to 0.12]	[-0.27 to 0.27]/[-0.20 to 0.20]
	Combined	0.00 / -0.01	[-0.15 to 0.15]/[-0.08 to 0.08]	[-0.21 to 0.21]/[-0.15 to 0.15]

Table 9: Summary of allowed 68% CL and 95% CL intervals on C_{uG} and C_{cG} effective coupling obtained in ee, $e\mu$, $\mu\mu$ and combined channels ($\Lambda = 1TeV$).

	68% exp./obs.limit	95% exp./obs.limit
σ(pp$\rightarrow$tW)$\times$B(W$\rightarrow \ell\nu$)^2	[0,0.10] /[0,0.03] pb	[0,0.20] /[0,0.11] pb
$C_{uG}(\Lambda = 1$ TeV)	[-0.07,0.07] /[-0.04,0.04]	[-0.10,0.10] /[-0.07,0.07]
B(t $\rightarrow$ ug)	[0,0.00243%]/[0,0.00087%]	[0,0.00491%]/[0,0.00270%]
σ(pp$\rightarrow$tW)$\times$B(W$\rightarrow \ell\nu$)^2	[0,0.13] /[0,0.04] pb	[0,0.26] /[0,0.13] pb
C_{cG} ($\Lambda = 1$ TeV)	[-0.15,0.15] /[-0.08,0.08]	[-0.21,0.21] /[-0.15,0.15]
B(t $\rightarrow$ cg)	[0,0.00314%]/[0,0.00101%]	[0,0.00643%]/[0,0.00325%]

Table 10: The expected and observed 95% CL upper limits on the cross section of tW production via C_{uG} and C_{cG} effective couplings times square of the branching fraction B(W$\rightarrow \ell\nu$), the effective couplings C_{uG} and C_{cG}, and the corresponding branching fractions B(t $\rightarrow$ ug) and B(t $\rightarrow$ cg).

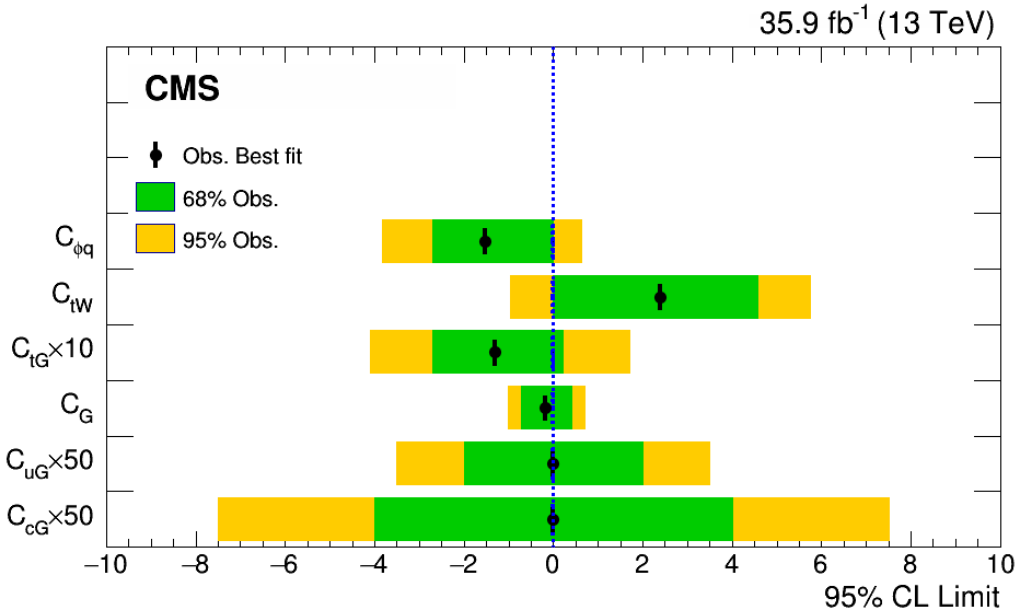

Figure 19: Observed and expected 95% CL upper limits on the top quark effective couplings for combined channel ($\Lambda = 1$ TeV).

11 Summary

This notes presents the search for new physics in top sector using events with two leptons and b jets in final state. Effective field theory approach is employed to find model independent results. In addition to the measurement of the SM tW cross section as a cross check, all sensitive related effective couplings are constrained at 95% CL.

References

[1] C. Zhang and S. Willenbrock, "Effective-Field-Theory Approach to Top-Quark Production and Decay", *Phys. Rev.* **D83** (2011) 034006, doi:10.1103/PhysRevD.83.034006, arXiv:1008.3869.

[2] G. Durieux, F. Maltoni, and C. Zhang, "Global approach to top-quark flavor-changing interactions", *Phys. Rev.* **D91** (2015), no. 7, 074017, doi:10.1103/PhysRevD.91.074017, arXiv:1412.7166.

[3] B. Grzadkowski, M. Iskrzynski, M. Misiak, and J. Rosiek, "Dimension-Six Terms in the Standard Model Lagrangian", *JHEP* **10** (2010) 085, doi:10.1007/JHEP10(2010)085, arXiv:1008.4884.

[4] P. L. Cho and E. H. Simmons, "Searching for G3 in $t\bar{t}$ production", *Phys. Rev.* **D51** (1995) 2360–2370, doi:10.1103/PhysRevD.51.2360, arXiv:hep-ph/9408206.

[5] D0 Collaboration, "Combination of searches for anomalous top quark couplings with 5.4 fb^{-1} of $p\bar{p}$ collisions", *Phys. Lett.* **B713** (2012) 165–171, doi:10.1016/j.physletb.2012.05.048, arXiv:1204.2332.

[6] ATLAS Collaboration, "Probing the Wtb vertex structure in t-channel single-top-quark production and decay in pp collisions at $\sqrt{s} = 8$ TeV with the ATLAS detector", *JHEP* **04** (2017) 124, doi:10.1007/JHEP04(2017)124, arXiv:1702.08309.

[7] ATLAS Collaboration, "Measurement of the W boson polarisation in $t\bar{t}$ events from pp collisions at $\sqrt{s}$ = 8 TeV in the lepton+jets channel with ATLAS", *Eur. Phys. J.* **C77** (2017), no. 4, 264, doi:10.1140/epjc/s10052-017-4819-4, arXiv:1612.02577.

[8] CMS Collaboration, "Search for anomalous Wtb couplings and flavour-changing neutral currents in t-channel single top quark production in pp collisions at $\sqrt{s} = 7$ and 8 TeV", *JHEP* **02** (2017) 028, doi:10.1007/JHEP02(2017)028, arXiv:1610.03545.

[9] CMS Collaboration, "Measurement of the W boson helicity in events with a single reconstructed top quark in pp collisions at $\sqrt{s} = 8$ TeV", *JHEP* **01** (2015) 053, doi:10.1007/JHEP01(2015)053, arXiv:1410.1154.

[10] CMS Collaboration, "Search for anomalous top chromomagnetic dipole moments from angular distributions in $t\bar{t}$ dileptonic events at $\sqrt{s} = 7$ tev with the cms detector", *CMS-PAS-TOP-14-005* (2014).

[11] D0 Collaboration, "Search for flavor changing neutral currents via quark-gluon couplings in single top quark production using 2.3 fb^{-1} of $p\bar{p}$ collisions", *Phys. Lett.* **B693** (2010) 81–87, doi:10.1016/j.physletb.2010.08.011, arXiv:1006.3575.

[12] CDF Collaboration, "Search for top-quark production via flavor-changing neutral currents in W+1 jet events at CDF", *Phys. Rev. Lett.* **102** (2009) 151801, doi:10.1103/PhysRevLett.102.151801, arXiv:0812.3400.

[13] ATLAS Collaboration, "Search for single top-quark production via flavour-changing neutral currents at 8 TeV with the ATLAS detector", *Eur. Phys. J.* **C76** (2016), no. 2, 55, doi:10.1140/epjc/s10052-016-3876-4, arXiv:1509.00294.

[14] A. Buckley et al., "Constraining top quark effective theory in the LHC Run II era", *JHEP* **04** (2016) 015, doi:10.1007/JHEP04(2016)015, arXiv:1512.03360.

[15] J. A. Aguilar-Saavedra, "A Minimal set of top anomalous couplings", *Nucl. Phys.* **B812** (2009) 181–204, doi:10.1016/j.nuclphysb.2008.12.012.

[16] https://cp3.irmp.ucl.ac.be/projects/madgraph/wiki/FAQ-General-13.

[17] D. Barducci et al., "Interpreting top-quark LHC measurements in the standard-model effective field theory", arXiv:1802.07237.

[18] http://feynrules.irmp.ucl.ac.be/attachment/wiki/TopEffTh/TopEffTh.fr#L230.

[19] D. Buarque Franzosi and C. Zhang, "Probing the top-quark chromomagnetic dipole moment at next-to-leading order in QCD", *Phys. Rev. D* **91** (2015), no. 11, 114010, doi:10.1103/PhysRevD.91.114010, arXiv:1503.08841.

[20] C. Zhang, "Single Top Production at Next-to-Leading Order in the Standard Model Effective Field Theory", *Phys. Rev. Lett.* **116** (2016), no. 16, 162002, doi:10.1103/PhysRevLett.116.162002, arXiv:1601.06163.

[21] s. Chenarani et al., "Measurement of the cross-section for tw production in dilepton final state at 13 tev using 2016 data", CMS Note 2017/132, 2017.

[22] http://feynrules.irmp.ucl.ac.be/wiki/GeneralFCNTop.

[23] J. Keaveney, M. Martin, M. Savitskyi, and G. Grohsjean, "Constraining effective field theories of new physics using top quark observables.", CMS Note 2017/088,TOP-17-014, 2017.